MATHEMATICAL MODELING OF THE MECHANICAL RESPONSE OF COUPLED INNER-EAR HAIR CELLS WITH OPPOSITE POLARITY

Mr. Tanawat Ngampattrapan

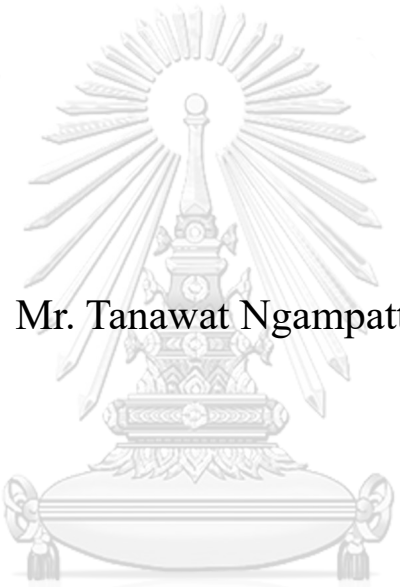

จุฬาลงกรณ์มหาวิทยาลัย
Chulalongkorn University

A Thesis Submitted in Partial Fulfillment of the Requirements
for the Degree of Master of Science in Physics
Department of Physics
FACULTY OF SCIENCE
Chulalongkorn University
Academic Year 2022
Copyright of Chulalongkorn University

จุฬาลงกรณ์มหาวิทยาลัย
Chulalongkorn University

แบบจำลองทางคณิตศาสตร์ของการตอบสนองเชิงกลของเซลล์ขนในหูชั้นในที่เชื่อมต่อกันแบบมีทิศทางตรงกันข้าม

นายธนวัฒน์ งามพัตราพันธุ์

จุฬาลงกรณ์มหาวิทยาลัย
CHULALONGKORN UNIVERSITY

วิทยานิพนธ์นี้เป็นส่วนหนึ่งของการศึกษาตามหลักสูตรปริญญาวิทยาศาสตรมหาบัณฑิต
สาขาวิชาฟิสิกส์ ภาควิชาฟิสิกส์
คณะวิทยาศาสตร์ จุฬาลงกรณ์มหาวิทยาลัย
ปีการศึกษา 2565
ลิขสิทธิ์ของจุฬาลงกรณ์มหาวิทยาลัย

Thesis Title	MATHEMATICAL MODELING OF THE MECHANICAL RESPONSE OF COUPLED INNER-EAR HAIR CELLS WITH OPPOSITE POLARITY
By	Mr. Tanawat Ngampattrapan
Field of Study	Physics
Thesis Advisor	Assistant Professor YUTTANA ROONGTHUMSKUL

Accepted by the FACULTY OF SCIENCE, Chulalongkorn University in Partial Fulfillment of the Requirement for the Master of Science

..... Dean of the FACULTY OF SCIENCE
(Professor POLKIT SANGVANICH)

THESIS COMMITTEE

..... Chairman
(Associate Professor NAKORN PHAISANGITTISAKUL)

..... Thesis Advisor
(Assistant Professor YUTTANA ROONGTHUMSKUL)

..... Examiner
(Assistant Professor RANGSIMA CHANPHANA)

..... External Examiner
(Associate Professor Chittanon Buranachai)

จุฬาลงกรณ์มหาวิทยาลัย
Chulalongkorn University

ธนวัตน์ งามพัตราพันธุ์ : แบบจำลองทางคณิตศาสตร์ของการตอบสนองเชิงกลของเซลล์ขนในหูชั้นในที่เชื่อมต่อกันแบบมีทิศทางตรงกันข้าม. (MATHEMATICAL MODELING OF THE MECHANICAL RESPONSE OF COUPLED INNER-EAR HAIR CELLS WITH OPPOSITE POLARITY) อ.ที่ปรึกษาหลัก : ผศ. ดร.ยุทธนา รุ่งธรรมสกุล

เซลล์ขนในหูชั้นในของสัตว์มีกระดูกสันหลังมีหน้าที่ตรวจจับแรงภายนอก เช่น เสียงในระบบการได้ยิน และความเร่งในระบบการทรงตัว โดยเซลล์ขนแต่ละเซลล์จะมีความไวต่อแรงในทิศทางหนึ่งๆเท่านั้น โดยทั่วไป เซลล์ขนในหูชั้นในจะถูกตรึงเข้ากับเนื้อเยื่อโดยรอบซึ่งทำหน้าที่เชื่อมต่อเซลล์ขนใกล้เคียงเข้าด้วยกัน งานวิจัยที่ผ่านมาได้นำเสนอแบบจำลองทางคณิตศาสตร์ที่ทำนายว่าการทำงานร่วมกันของเซลล์ขนสามารถเพิ่มความไวต่อสัญญาณภายนอกได้ งานวิจัยดังกล่าวศึกษาการทำงานร่วมกันของเซลล์ขนที่มีทิศทางเดียวกัน ซึ่งเป็นแบบจำลองของกลุ่มเซลล์ขนในระบบการได้ยิน อย่างไรก็ตาม ในปัจจุบันยังไม่มีการศึกษาผลจากการเชื่อมต่อกันของเซลล์ขนที่สามารถตรวจจับแรงในทิศทางตรงกันข้ามกัน ซึ่งเป็นรูปแบบการจัดเรียงเซลล์ขนในระบบการได้ยินของกิ้งก่ารวมทั้งระบบการทรงตัวของสัตว์มีกระดูกสันหลังทุกชนิด ในงานวิจัยนี้เรามุ่งศึกษาพลวัตของเซลล์ขนสองเซลล์ที่สามารถตรวจจับแรงในทิศทางตรงข้ามกันที่มีการเชื่อมต่อกันด้วยสปริงโดยใช้แบบจำลองทางคณิตศาสตร์ที่ปรับปรุงจากแบบจำลองที่อธิบายการทำงานของเซลล์ขนเดี่ยว โดยศึกษาการเคลื่อนที่ของระบบเซลล์ในสามกรณี ได้แก่ กรณีไม่มีแรงภายนอก กรณีที่ระบบถูกกระทำโดยแรงรูปไซน์ และกรณีที่ระบบถูกกระทำโดยแรงแบบขั้นบันได จากการวิเคราะห์ผลจากแบบจำลองโดยวิธีเชิงตัวเลขพบว่า เราสามารถพิจารณาระบบเป็นเซลล์ขนเดี่ยวที่ถูกกระทำโดยแรงเนื่องจากสปริงที่เชื่อมต่อเซลล์ขนทั้งสอง ซึ่งส่งผลต่อจุดปฏิบัติการ (Operating point) ของเซลล์ โดยทำให้ระบบสามารถเกิดการสั่นได้เองได้ง่ายขึ้น ในกรณีที่ระบบของเซลล์ขนถูกกระทำโดยแรงภายนอกรูปไซน์ พบว่าแรงจากการเชื่อมมีขนาดเปลี่ยนแปลงกับเวลาด้วยความถี่เป็นสองเท่าของแรงภายนอก แรงดังกล่าวส่งผลต่อขนาดของการตอบสนองที่ความถี่ของแรงภายนอก โดยการลดการตอบสนองเมื่อแรงภายนอกมีแอมปลิจูดสูงหรือมีความถี่น้อยกว่าความถี่มูลฐานของเซลล์ ปรากฏการณ์นี้บ่งชี้ว่าการตอบสนองของระบบมีความไม่เชิงเส้นสูงขึ้น นอกจากนี้ยังอาจเพิ่มความสามารถในการแยกแยะความถี่ของเซลล์ขนได้อีกด้วย นอกจากนี้ เราพบว่าการเชื่อมต่อของเซลล์มีผลต่อขนาดการตอบสนองต่อแรงแบบขั้นบันได โดยเพิ่มขนาดการตอบสนองต่อแรงในทิศทางของการเปิดช่องไอออนของเซลล์ และลดขนาดการตอบสนองต่อแรงในทิศทางปิดช่องไอออน งานวิจัยนี้เพิ่มพูนความเข้าใจในการเชื่อมต่อระหว่างเซลล์ขนซึ่งอาจมีส่วนสำคัญในการตรวจจับแรงภายนอกของระบบทรงตัวและหูชั้นในของกิ้งก่า

จุฬาลงกรณ์มหาวิทยาลัย
CHULALONGKORN UNIVERSITY

สาขาวิชา	ฟิสิกส์	ลายมือชื่อนิสิต .....
ปีการศึกษา	2565	ลายมือชื่อ อ.ที่ปรึกษาหลัก .....

6370220223 : MAJOR PHYSICS
KEYWORD: Biological Physics, Auditory System, Nonlinear Oscillators, Hair cell Polarity

Tanawat Ngampattrapan : MATHEMATICAL MODELING OF THE MECHANICAL RESPONSE OF COUPLED INNER-EAR HAIR CELLS WITH OPPOSITE POLARITY . Advisor: Asst. Prof. YUTTANA ROONGTHUMSKUL

Hair cells are specialized receptors that detect mechanical forces in the auditory and vestibular systems of vertebrates. *In vivo* hair-cell bundles are typically anchored to an overlying structure which provides mechanical coupling between neighboring hair cells. Cooperativity between hair bundles has been previously proposed to have strong effects on signal detection. While the coupling of hair cells with the same polarity as those in the auditory organs has been extensively studied, the dynamics of hair cells with opposite polarity in the vestibular system and the inner ear of lizards remain unexplored. In this study, we aim to investigate the dynamics of two hair cells arranged with opposite polarity under a coupling spring using a mathematical model previously proposed to describe hair bundle motility. We focused on three scenarios: spontaneous dynamics, responses to sinusoidal force stimulation, and responses to step force stimulation. Through our analyses, we showed that the coupling force applied to each hair cell by the coupling element served as an additional force that modulated the individual cell's dynamics. Notably, when coupled with opposite polarity, the coupling force counteracted the applied constant force, which affected the hair cell's operating point. Under sinusoidal force stimulation, the coupling force oscillated at twice the frequency of the driving force. This oscillatory force could affect the response of the coupled hair bundle at the driving frequency, leading to reduced responses at high force amplitudes and frequencies below the resonance frequency. This phenomenon could improve the hair cell's compressive nonlinearity and frequency selectivity. Furthermore, we observed that the coupling force increased the responses to positive step forces while decreasing responses to negative forces. Our study contributes to the understanding of coupled hair-bundle dynamics which could play important roles in the signal detections by the vestibular systems and inner ear of lizards.

จุฬาลงกรณ์มหาวิทยาลัย
CHULALONGKORN UNIVERSITY

Field of Study: Physics Student's Signature .....
Academic Year: 2022 Advisor's Signature .....

ACKNOWLEDGEMENTS

I would like to express my deep appreciation to my advisor, Asst.Prof.Dr. Yuttana Roongthumskul, for his unwavering patience, guidance, and support throughout the long journey of this thesis. His expertise and mentorship have been invaluable, and I am grateful for his dedication and encouragement throughout the years in this course.

I would also like to extend my thanks to all the staff from the Department of Physics for their helpful advice and assistance regarding the various regulations involved in submitting this thesis. Their support has been instrumental in navigating the administrative aspects of this research endeavor.

Furthermore, I would like to express my gratitude to everyone in the OAEs group for their valuable insights and advice in the field of study. Their contributions have greatly enriched my research and broadened my understanding of the subject matter.

Finally, I would like to acknowledge and thank my friends at the Department of Physics for their continuous encouragement and motivation. Their unwavering support has been a driving force in helping me complete this thesis.

Tanawat Ngampattrapan

จุฬาลงกรณ์มหาวิทยาลัย
Chulalongkorn University

TABLE OF CONTENTS

Page

ABSTRACT (THAI) iii
ABSTRACT (ENGLISH) iv
ACKNOWLEDGEMENTS v
TABLE OF CONTENTS vi
LIST OF FIGURES viii
Chapter 1 Introduction 1
1.1 Background and motivations 1
1.2 Objectives 3
1.3 Scope of thesis 3
1.4 Research procedures 3
1.5 Expected benefits 5
1.6 Overall 5
Chapter 2 Background Theory 7
2.1 Hair bundle's structure and mechanical Properties 7
2.2 Hair cell orientation 10
2.3 Effects of overlying structures 11
2.4 Mathematical model of hair-bundle motility 13
2.5 Predictions from the model 15
2.6 Phase portrait of a nonlinear oscillator 17
Chapter 3 Methodology 19
3.1 Mathematical model of a single hair bundle 19
3.2 Model of coupled hair bundles 20
3.3 Numerical simulation and frequency analysis 20
3.4 Parameters value 21
3.5 Calculation of the constant force experienced by coupled hair bundles 23

จุฬาลงกรณ์มหาวิทยาลัย
Chulalongkorn University

Chapter 4 Results 25
4.1 Spontaneous dynamic 25
4.2 Responses to sinusoidal force 30
4.3 Responses to step force 44
Chapter 5 Discussion and Conclusion 55
5.1 Discussion 55
5.2 Suggestions and future work 57
REFERENCES 59
VITA 62

จุฬาลงกรณ์มหาวิทยาลัย
Chulalongkorn University

LIST OF FIGURES

Page

Figure 1.1 Schematic diagram of hair bundles. 1
Figure 1.2 Schematic diagram of the cross section of the inner ear of tokay geckos. .. 2
Figure 2.1 Schematic diagram of hair cell. 7
Figure 2.2 The gating of hair bundle when receiving a force in direction of taller villi. 8
Figure 2.3 Nonlinearity of hair bundle..... 9
Figure 2.4 Orientation and overlying structure of hair cells in various organs. 11
Figure 2.5 Operating points suitable on detecting different kind of force of hair bundle..... 13
Figure 2.6 Spontaneous oscillation and state diagram of hair bundle. 16
Figure 2.7 Responses of hair bundle to external force..... 17
Figure 2.8 Phase portrait of equation (2.2) at 3 different sets of parameters. 18
Figure 3.1 Schematic diagram of coupled oscillator. 20
Figure 3.2 Step force to time..... 21
Figure 3.3 Force-displacement relation from the model. 23
Figure 4.1 State Diagram for coupled oscillators. 26
Figure 4.2 Peak-to-peak amplitude of coupled oscillators with opposite polarity..... 29
Figure 4.3 Force acting on individual oscillator. 30
Figure 4.4 Sensitivity of coupled oscillators with identical polarity..... 32
Figure 4.5 Sensitivity plot vs driving force frequency for coupled oscillator with opposite polarity..... 33
Figure 4.6 Sensitivity vs driving force frequency of coupled oscillators with opposite polarity at the same operating point..... 34
Figure 4.7 Sensitivity of coupled oscillators at frequency of 0.0675 and driving force amplitude of 0.1. 35
Figure 4.8 Plot of sensitivity versus driving force amplitude for coupled oscillators 37

Figure 4.9 Comparison between the displacements of a coupled oscillator and a single oscillator 38
Figure 4.10 Coupling force. 39
Figure 4.11 Power spectrum of responses from 3 different cases. 39
Figure 4.12 Sensitivity of a single oscillator vs phase of the second harmonic force 41
Figure 4.13 Phase of extracted coupling force. 42
Figure 4.14 Ratio between the amplitude of the coupling force and the driving force. 43
Figure 4.15 Sensitivity at off-resonance frequencies. 44
Figure 4.16 Schematic diagram of coupled oscillator with opposite polarity receiving a positive step force with respect to the first oscillator. 45
Figure 4.17 Responses to step force of coupled oscillators with identical polarity 46
Figure 4.18 Responses of oscillators with opposite polarity. 47
Figure 4.19 Trajectory of the oscillator receiving the step force 49
Figure 4.20 Trajectory of the oscillator shown in Figure 4.17 in phase plane. 50
Figure 4.21 Trajectory and nullcline of each oscillator. 52
Figure 4.22 Responses of coupled oscillators to step force at higher Kc 53
Figure 4.23 Coupling force and the total force acting on each oscillator for Kc= 1. .54

จุฬาลงกรณ์มหาวิทยาลัย
Chulalongkorn University

Chapter 1
Introduction

1.1 Background and motivations

Auditory and vestibular systems of vertebrates are able to detect external forces with high sensitivity and frequency selectivity. These systems utilize hair cells whose sub-cellular structures comprise of packed villi arranged in graded height, called the hair bundle, to perceive the incoming forces (Figure 1.1). This structure gives rise to an asymmetry in the activation of the hair bundle: a deflection in the direction toward the taller villi results in the opening of mechanically gated ion channels on the hair bundle, whereas the deflection toward the shorter villi closes the channels [1]. This directional activation of a hair bundle is referred to as hair bundle polarity. The gating of ion-channels generates nerve signals sent to the brain resulting in a perception of the external forces.

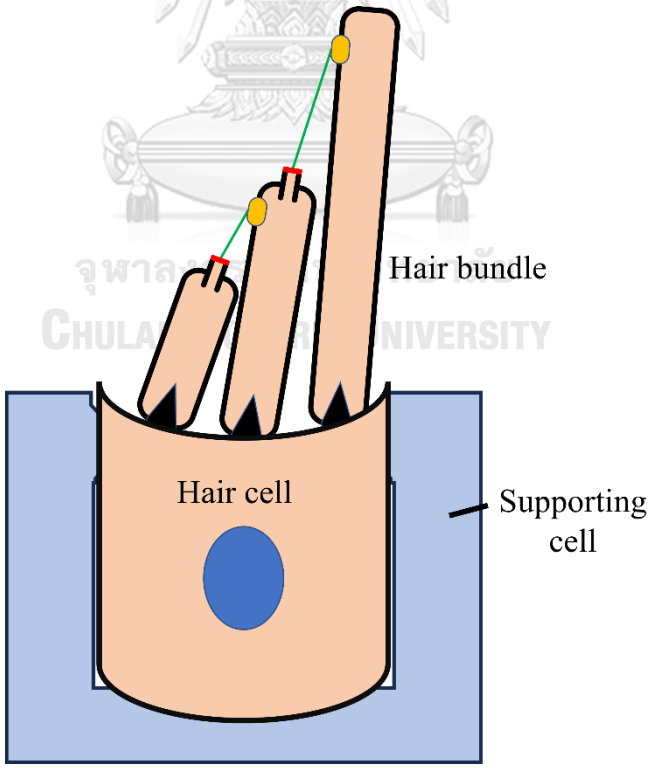

Figure 1.1 Schematic diagram of hair bundles. Adapted from [1].

Hair cells in vestibular system and auditory system perceive different kinds of forces. The vestibular system is responsible for the detection of body movement and orientation while the auditory system is responsible for detecting sounds. There are several suggestions that the hair cell's ability to sense distinct types of stimuli is governed by the *in vivo* auxiliary structures that imposed different mechanical loads on hair bundles [2-4]. Theoretical predictions suggest that the stiffness of the mechanical load and the constant force imposed on hair bundles can tune hair bundles to different operating points within a state diagram suitable for the detection of a specific type of forces [2].

However, *in vivo* hair bundles are also mechanically connected via an overlying membrane, and thus potentially operate in groups. Investigations of the anatomy of the vertebrate inner ears reveal that *in vivo* hair bundles of the auditory organs, such as the mammalian cochlea, are often arranged with identical polarities [5, 6]. On the other hand, hair bundles in the vestibular organs, such as the semicircular canal, the saccule, and the fish lateral line, are arranged primarily with opposing polarities. An exception includes the auditory organs of several lizard species that incorporate hair bundles with opposite polarities (Figure 1.2) [6].

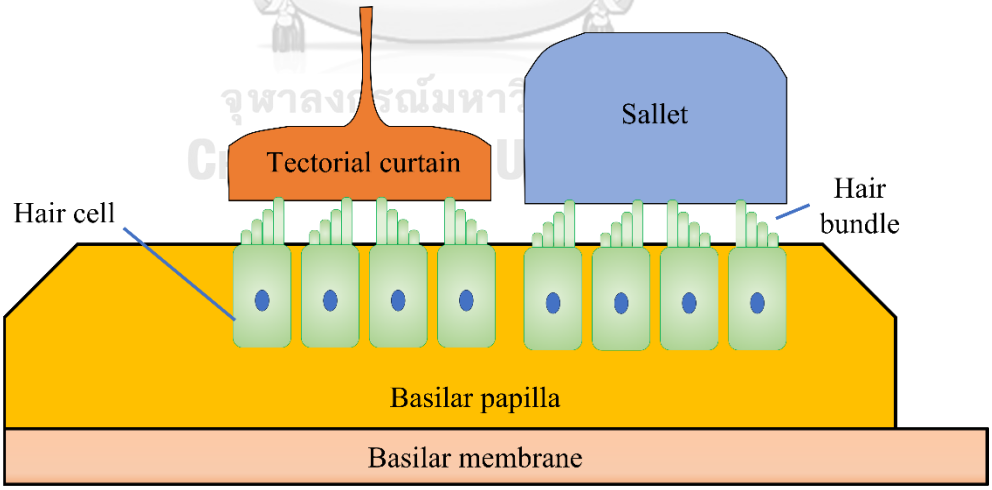

Figure 1.2 Schematic diagram of the cross section of the inner ear of tokay geckos.Hair bundles are covered by sallet or tectorial curtain. In each group, hair bundles are coupled together with opposite polarities adapted from [6].

Hair bundles are anchored to an overlying tissue *in vivo*, a structure which provides mechanical coupling between neighboring hair bundles. Previous theoretical

investigations suggest that a group of coupled hair bundles, arranged with identical polarities, can display an enhanced mechanical sensitivity and a lower detection threshold, consistent with experimental findings in two or three coupled hair bundles [7-11]. However, it remains unknown whether coupling of hair bundles with opposite polarities, an organization ubiquitously found in the vertebrate vestibular system and lizard auditory organs, benefits the detection of mechanical signals. In the mammalian cochleae, the low detection threshold, i.e., 0 decibel, and high frequency selectivity of hair cells are facilitated by electromotility. This process is mediated by prestin protein that causes the hair cell body to contract or elongated upon changes in its membrane electric potential [6]. Although hair cells within the lizard inner ears do not display electromotility, their hearing thresholds are comparable to those of mammals. This raises the question whether the polarities of hair cells in the inner ear of lizards could serve as an amplification process as the electromotility process in mammals.

This thesis aims to study the effects of opposite polarity on the mechanical response of coupled hair cells. We performed numerical simulations of the mathematical model previously proposed to describe the dynamics of single hair bundles [2] to study the mechanical responses of coupled hair bundles with opposite polarity to external sinusoidal forces and step forces.

1.2 Objectives

1.1.1 To investigate the spontaneous dynamics of hair bundles coupled with opposite polarities.

1.1.2 To investigate the effects of hair bundle's polarity on the responses to sinusoidal forces and step forces.

1.3 Scope of thesis

Numerical simulations of the model from [2] will be performed. The parameters will be based on [2]. We only consider the effects of coupling two hair bundles with identical parameters.

1.4 Research procedures

1.4.1 Literature review

จุฬาลงกรณ์มหาวิทยาลัย
CHULALONGKORN UNIVERSITY

We will review the mathematical models of hair bundle motility, which are based on the physiology of transduction channels and other mechanisms within the hair bundle. Additionally, we will explore theoretical models that describe a hair bundle as a nonlinear oscillator near a Hopf bifurcation. Subsequently, we will investigate the functions of hair bundles and analyze their response when poised at different operating points. Finally, we will examine the effects of mechanical coupling between hair bundles on their dynamics, including factors such as the signal-to-noise ratio, quality factor, sensitivity, and frequency selectivity in response to sinusoidal forces.

1.4.2 Investigation of the dynamics of single hair bundles in response to external forces and comparison to literature.

We perform the numerical simulation of the mathematical model based on [2] by implementing the model on MATLAB. We will compare the spontaneous dynamics of a single hair bundle and its responses to external forces to literatures.

1.4.3 Develop a model of two coupled hair bundles based on [2].

A mathematical model of two coupled hair bundles will be developed. Coupling will be mediated by a mechanical spring. The equations of motion for individual hair bundles are based on (1.1) as follows

จุฬาลงกรณ์มหาวิทยาลัย
Chulalongkorn University

$$m\ddot{x}_i = -\gamma\dot{x}_i - kx_i + a(x_i - f_i) - (x_i - f_i)^3 + F_i - K_c\left(x_i - Px_j\right) \quad (1.1)$$

$$\tau\dot{f}_i = bx_i - f_i$$

where x represents the displacement of the hair bundle, and an internal parameter, f, representing the force from a myosin motor complex, m denotes the mass of the hair bundle, and γ denotes a damping coefficient. The stiffnesses of the system are denoted by k, and a, the latter corresponds to the gating of ion channels. Each oscillator is under external forces, $F.\ i$

and j = 1,2 with $i \neq j$. P indicates the polarity of the two bundles, with P= 1 if they have the same polarity and P = -1 if they have opposite polarities.

1.4.4 Investigation of the spontaneous dynamics of coupled hair bundles.

By fixing the stiffness and constant force on each bundle, we will vary the coupling stiffness and investigate the spontaneous dynamic of the coupled hair bundles.

1.4.5 Investigation of the responses of coupled hair bundles to external forces.

1) We will include the external force term in equation (1.1), with a sinusoidal force or a step force. Investigate the responses of coupled hair bundle at fixed operating point of each hair bundle near the Hopf bifurcation in quiescence regime.

2) Calculate the sensitivity of coupled hair bundles subjected to sinusoidal force and analyzed the effects of coupling force to responses of hair bundles. The responses to step force will be studied by observing the trajectory of hair bundle in phase plane and analyzed the effects of coupling force.

1.4.7 Conclusion and writing the thesis.

จุฬาลงกรณ์มหาวิทยาลัย
Chulalongkorn University

1.5 Expected benefits

Investigation of the effects of polarity on the dynamics of coupled hair bundles will provide further insight knowledge on signal detections by the vertebrate vestibular system, as well as the lizards' auditory system.

1.6 Overall

The following chapter is a background theory about the structure and properties of hair cells and orientations *in vivo* and the mathematical model of hair cells. In chapter 3, we introduce the mathematical model of coupled hair cells and methods to analyze the results from simulations. In chapter 4, we present the results of numerical simulation of coupled hair cells in three cases, no external force, subject to sinusoidal

force, and subject to step force. Finally, chapter 5 will discuss the results then deliver a summary and suggestions from the thesis.

จุฬาลงกรณ์มหาวิทยาลัย
Chulalongkorn University

Chapter 2

Background Theory

2.1 Hair bundle's structure and mechanical Properties

Hair cells are mechanical force receptors found in the vestibular system and auditory system of vertebrates. The primary function of hair cells is to transform the external mechanical force into electrical signals that are subsequently sent to the brain. The structure of a hair cell can be divided into 2 main parts, the cell body, and the hair bundle (Figure 2.1). The cell body is embedded in the epithelium of the sensory organ and connected to the auditory nerves. This part of the cell transforms the mechanical force into a nerve signal. The hair bundle is a group of villi called stereocilium packed together with graded height, situated on top of the hair cell's body (Figure 2.1). Each villus is connected to its nearest neighbor through a tip link. The lower end of the tip link is connected to one or two mechanically gated ion-channels, situated at the top of the shorter villus, and the upper end of the tip link is connected to the insertional plague which comprises of myosin motors on the side of the taller villus.

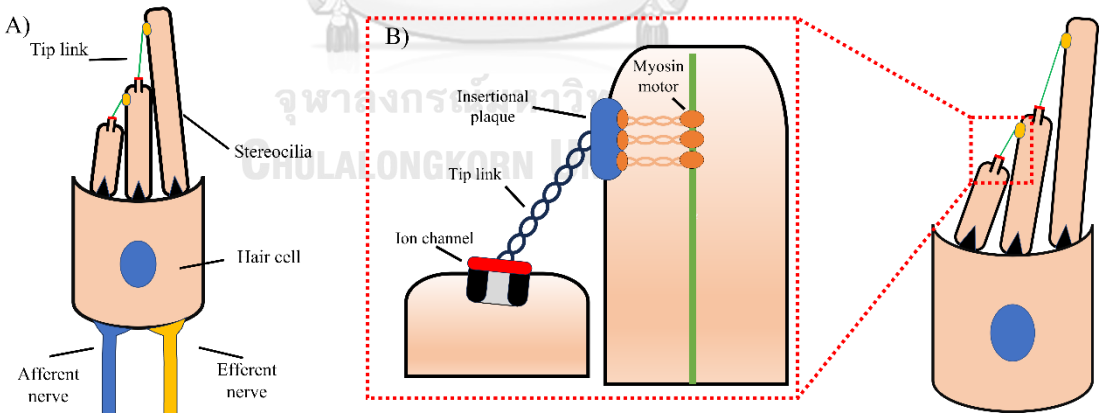

Figure 2.1 Schematic diagram of hair cell. A) shows schematic diagram of a hair cell, consisting of the cell body innervated by nerve fibers and the hair bundle situated on top of cell body which functions as force detector. B) a close-up image of a top of stereocilia shows the connection between ion channel, Tip link, and insertional plaque. Adapted from[1]

Force detection performed by the hair bundle relies on the gating of the ion-channels on top of the stereocilia. A force that deflects the bundle in the direction

toward the taller villi stretches the tip links owing to the graded height structure of the hair bundle. This raises the tension of the tip link which pulls the mechanical gating ion-channel open allowing the cation outside to flow inside the bundle (Figure 2.2). This increases hair-cell membrane's electrical potential and evokes neurotransmitter release at the synapse resulting in a nerve signal transmitted to the brain. For the force in the opposite direction, the hair bundle movement causes the ion channels to close and decreases the cation influx.

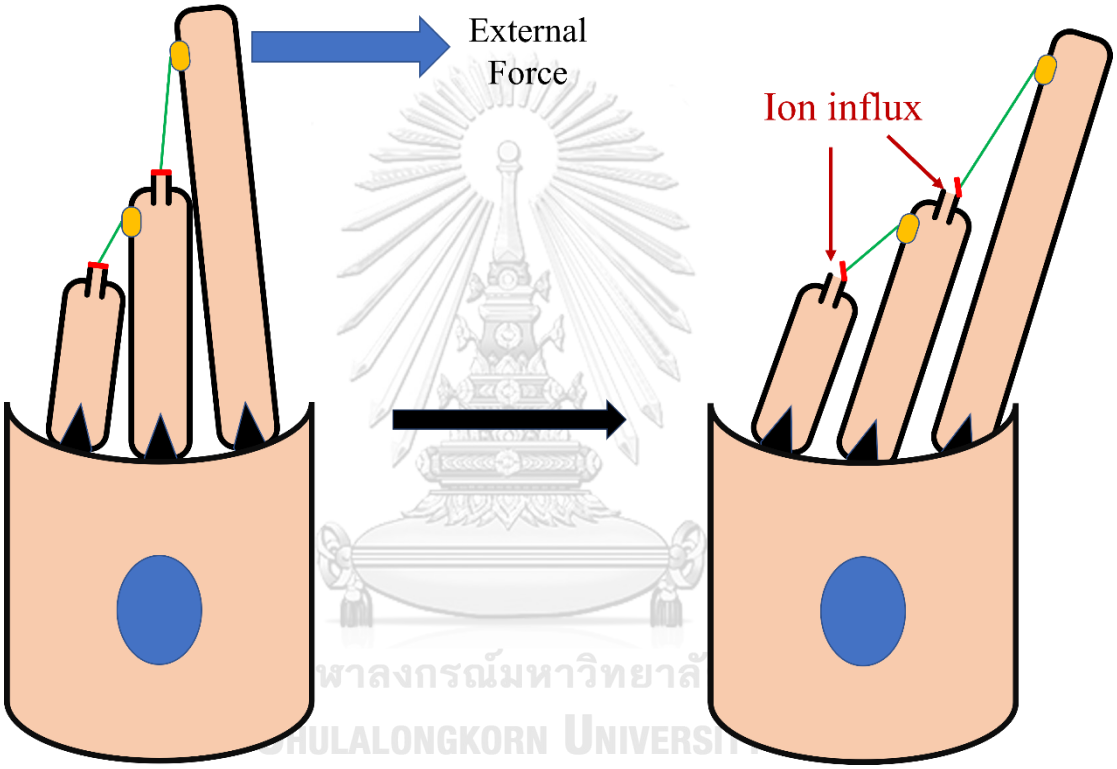

Figure 2.2 The gating of hair bundle when receiving a force in direction of taller villi. Due to the graded-height structure of hair bundle, the deflection causes tension Tip link and gating spring promote the open of ion-channels.

Hair bundles possess unique mechanical properties that attract the attentions of many researchers. Hair cells are able to detect weak external forces whose amplitudes are within the order of thermal noise and discriminate the forcing frequency with high resolutions. A hair cell operates a broad range of stimulus amplitude as it can detect a forcing amplitude over six orders of magnitude. These properties rely on the mechanical properties of the force receptor part of the hair cell, the hair bundle.

The underlying mechanisms of hair bundles' mechanical properties have been studied extensively. The ion channels on the stereocilia are mechanically gated [1, 5] which respond to applied mechanical force. Ion channels can be in an open or a close state with the probabilities described by a Boltzmann distribution [5] (Figure 2.3A). The ion channel is connected to a tip link which serves as a mechanical spring, called a gating spring [5]. Upon an application of a force in the direction toward the taller rows of the stereocilia, the gating spring extends causing the gate of the ion channel to swing open. This swing is associated with a decrease in the extension, as well as the tension, in the gating spring, causing the hair bundle to move further in the direction of the external force. This phenomenon is referred to as the gating compliance which effectively reduces the hair bundle's stiffness and causes the nonlinearity in force-displacement relation of single hair bundles [12] (Figure 2.3B). Under suitable chemical conditions, the force from the gating swing is greater and further reduces the bundle's stiffness until it eventually becomes negative (Figure 2.3C). This process gives rise to two equilibrium positions of a hair bundle, associated with an open and a closed state of the ion channels, instead of one stable position at the origin. For a displacement further away from the origin, the influence from gating swing is minimized. The stiffness of hair bundle is thus governed by the sum of the stiffnesses from the gating springs and the innate elastic elements of the hair bundle.

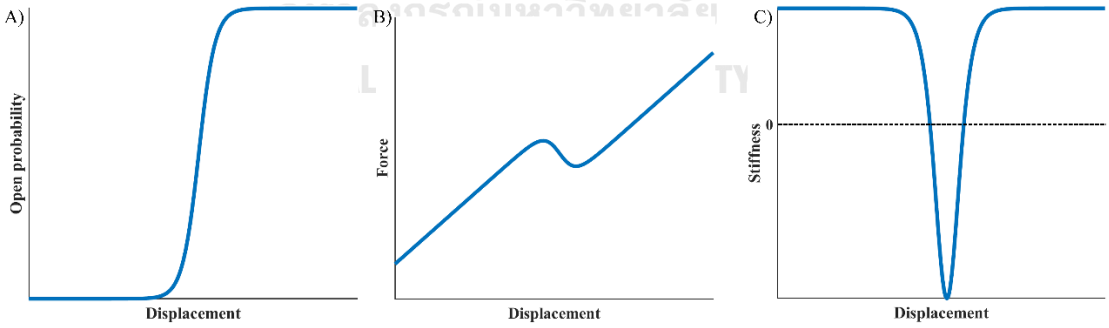

Figure 2.3 Nonlinearity of hair bundle. A) the open probability of ion channels which display a Boltzmann distribution. B) shows the nonlinearity of the force-displacement relation of hair bundle around x_0. C) the stiffness acquired from B) shows the reduction of stiffness at the nonlinear regime. When force from gating swing is high (dash line), it increases the nonlinearity in force-displacement relation, resulting in a greater drop in stiffness and eventually become negative.

Another crucial part of the hair bundle's internal mechanisms lies in the upper end of each tip link, called the insertional plague. For hair bundles to remain sensitive

to external force, the hair bundle has a mechanism that tries to adjust the open probability at an optimal value [5]. The insertional plaque is connected to a cluster of myosin motors which are attached to actin filaments inside the stereocilia. When ion channels open due to a positive force, calcium ions flow into the bundle and bind to myosin motors causing the reduction in the binding probability of the myosin motors to the actin filaments. The insertional plague consequently slides down along the side of stereocilia due to the downward force exerted by the gating spring. This action decreases the tension in the gating spring which promotes the closure of ion channels. On the other hand, when subjected to a negative force, the ion channels are closed which reduces the influx of calcium ions. The binding probability of myosin motors to the active filaments then increases the rate of myosin motors climbing upward along the acting filaments. This raises the tension in the gating spring and promotes the opening of ion channels. This movement also plays an important role in the spontaneous oscillations of hair bundle [13].

2.2 Hair cell orientation

Hair cells in the inner ear are often accompanied by nearby hair cells and accessory structures which provide coupling force and impose a stiffness load to the hair cells [5, 6]. In various sensory organs, hair cells are arranged with certain orientations. For the inner ears of mammals and avians, hair cells in their cochleae are often arranged with identical polarity, i.e., an external force can activate the ion channels in all hair bundles. These hair cells are coupled together through an overlying tectorial membrane (Figure 2.4A). The inner ears of some lizard species, however, incorporate hair cells that are divided into two groups with different overlying structures, one is a small membrane, called sallet, each coupling a row of hair cells, and the others is a tectorial curtain composed of a continuous membrane that couples all hair cells throughout the cochlea (Figure 2.4B). Hair cells under each sallet or tectorial membrane are arranged with opposite polarities, suggesting that an external force can activate only half of the hair bundles in the cochlea, while the ion channels of the other half will be suppressed.

In the vestibular system, hair cells are often arranged with opposite polarities. Hair cells in the literal line system of fishes and semicircular canals in mammals are

arranged in opposite directions and embedded in an overlying gel-like matrix termed cupula (Figure 2.4C). Hair cells in the utricles and saccules are coupled through an otolithic membrane [5].

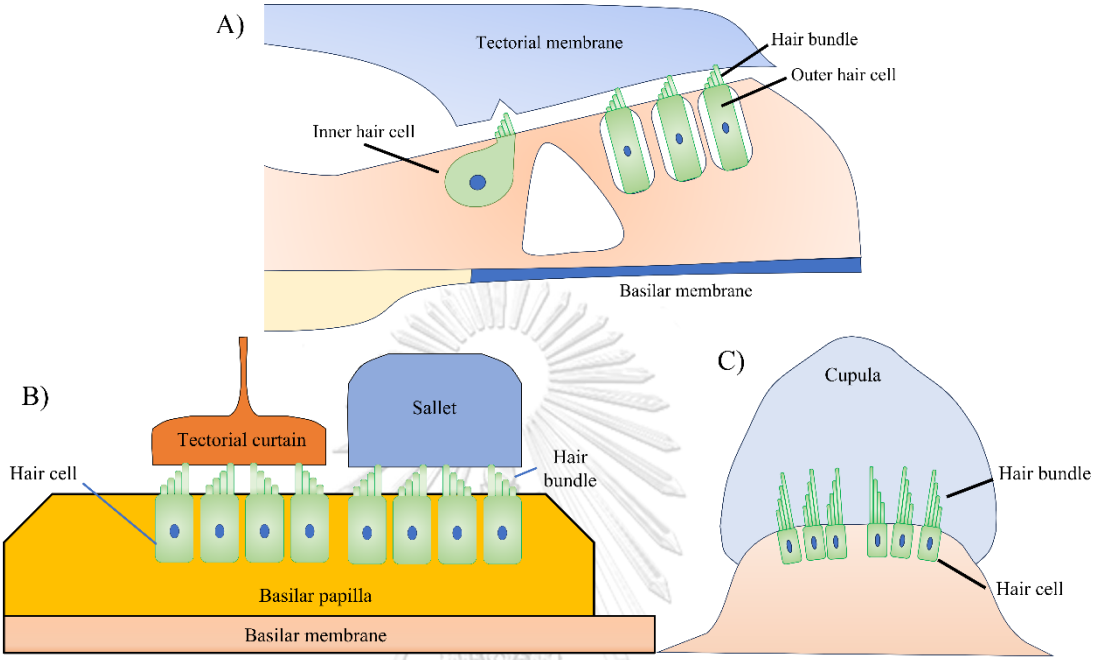

Figure 2.4 Orientation and overlying structure of hair cells in various organs. A) the cochlea in chicken and rat. B) the basilar papilla in lizard. Adapted from [6]. C) the hair bundle in semicircular canal. Adapted from [5].

2.3 Effects of overlying structures

The effects of mechanical coupling between hair bundles have been studied both theoretically and experimentally [7-11, 14, 15]. Theoretical models of hair bundle motility suggest several benefits of coupling hair bundles via a mechanical spring. First, hair bundles gain enhanced sensitivity to external sinusoidal force. Increasing the numbers of hair bundles in the system further improves the effects. Second, coupling improves the coherence of spontaneous oscillations of hair bundles. This is also associated with the enhanced frequency selectivity in response to sinusoidal forces. Finally, coupling can facilitate synchronization of hair bundles' spontaneous oscillations and reduced the impact of external noise [14, 15]. When the natural frequencies of the two coupled hair bundles diverge, spontaneous oscillation can be suppressed, and the detection thresholds and the signal-to-noise ratio can be improved [10].

There are multiple experimental studies on the effects of coupling on hair bundles *in vitro*. To study hair bundles *in vitro*, the overlying membrane is removed, and the hair cells are bathed in an appropriate solution. To imitate the coupling between hair bundles, there is an experiment that couple a hair bundle from the bullfrog sacculus to a mechanical actuator whose movement is governed by a mathematical model of hair bundle motility [13]. The results indicate that coupling to a virtual hair bundle can readily improve the coherence of spontaneous oscillations and the responses to external sinusoidal forces and reduce the noise level. Later experiments on two hair bundles coupled through an elastic fiber or a glass bead suggest similar results [11].

The effects of coupling hair bundles with opposite polarities have not been previously studied. However, it has been proposed based on the hearing threshold of lizards that this could enhance the sensitivity of the bundles in response to sinusoidal forces [16]. An additional study also reveals that coupled hair bundles with opposite polarity potentially display spontaneous oscillations *in vivo* [17].

The overlying structures do not only provide coupling between hair cells but also impose a stiffness load and constant forces onto hair bundles. It has been proposed that these mechanical loadings may adjust the stability of a hair bundle which has a central role in tuning the bundle to detect different types of forces [2-4]. Theoretical predictions suggest that without an external force, a hair bundle can appear in 3 states, spontaneously oscillating, quiescent, and bi-stable states. Each state is divided by a line of bifurcation shown in Figure 2.5. The stiffness and constant force loaded on a hair bundle can control the behavior of a hair bundle [2, 5]. For the auditory system, it has been suggested that hair bundles should have higher stiffnesses and be placed near a supercritical Hopf bifurcation. The hair bundle in this state displays an enhanced response to sinusoidal forces and frequency tuning. Hair bundles of the vestibular system should possess lower stiffnesses and operate near a subcritical Hopf bifurcation. The hair bundle's response to an external step force can display a large initial swing that goes beyond a stable displacement before swinging back to a stable point, suggesting its sensitivity to the onset of a step force.

จุฬาลงกรณ์มหาวิทยาลัย
Chulalongkorn University

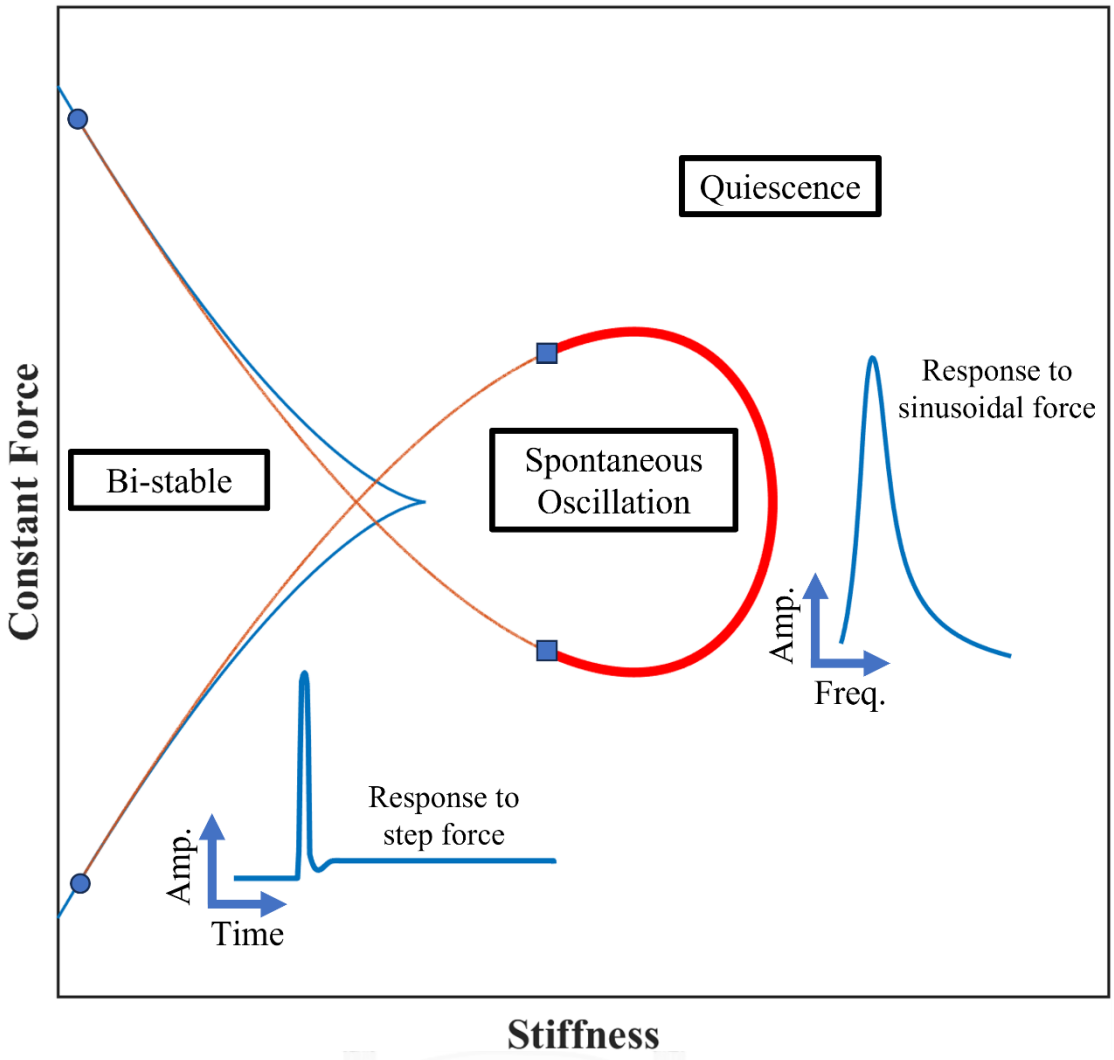

Figure 2.5 Operating points suitable on detecting different kind of force of hair bundle. For hair bundle near supercritical Hopf bifurcation (right side of state diagram), hair bundle responses to sinusoidal force with resonance behavior with higher quality factor near the line of Hopf bifurcation. On the other hand, the hair bundle near subcritical Hopf bifurcation responses with a twitch-like movement which suitable for onset detection for step force. Adapted from [5]

จุฬาลงกรณ์มหาวิทยาลัย
CHULALONGKORN UNIVERSITY

2.4 Mathematical model of hair-bundle motility

The dynamics of single hair bundles has been described by two types of mathematical models. First, the models that account for all the physiological processes of a hair bundle such as ion-channel gating mechanism and the dynamics of myosin motor [13]. The other type of models considers individual hair bundles as a nonlinear oscillator [2, 14, 15, 18].

The model of coupled hair bundles used in this thesis is based on a previously proposed model of a hair bundle [2]. The model can be derived from the equation of motion that governs the dynamics of a hair bundle under a mechanical loading, which imposes additional stiffness and a constant force on the hair bundle. The dynamics of the hair bundle are described by two coupled differential equations as follows.

$$M\ddot{X} = -(\Gamma + \Gamma_{hb})\dot{X} - \left(K_e + K_{sp}\right)X + A(X - \alpha F_a) - C(X - \alpha F_a)^3 + F \qquad (2.1)$$
$$D\dot{F}_a = BX - EF_a$$

where X is displacement of hair bundle, Γ is damping coefficient of the mechanical loading, Γ_{hb} is damping coefficient of hair bundle, K_e is stiffness imposed by the mechanical loading, K_{sp} is stiffness of pivot of villi, and F is external force. The terms $A(X - \alpha F_a) - C(X - \alpha F_a)^3$ approximate the gating force mediated by the gating spring which incorporates the negative stiffness due to gating of the ion channels (Figure 2.3). The term $X - \alpha F_a$ represents the extension of the gating spring determined by the bundle's position, X, and the position of the upper end of the tip link, which is written as αF_a. The variable F_a is the force exerted on the tip link by myosin motors, and α is a compliance corresponding to the reciprocal of the tip link stiffness. The parameters A has a unit of a stiffness, and C represents the strength of nonlinearity.

[2] approximates the force from myosin motor by a first-order differential equation, in which D is a constant that controls the relaxation time of myosin motor, B is the coupling coefficient between hair bundle displacement and myosin motor, and E determines the effect of myosin motor's own relaxation. The parameters in equation (2.1) are rescaled as follows.

$$\begin{array}{lll} x = C^{1/3}X & m = \frac{MC^{1/3}}{\Gamma_{hb}^2} & \gamma = 1 + \frac{\Gamma}{\Gamma_{hb}} \\ f = \alpha C^{1/3}F_a & a = \frac{A}{C^{1/3}} & k = \frac{K_e + K_{sp}}{C^{1/3}} \\ t = \frac{C^{1/3}}{\Gamma_{hb}}T & \tau = \frac{DC^{1/3}}{\Gamma_{hb}E} & b = \frac{B\alpha}{E} \end{array} \qquad (2.2)$$

The equations then become.

$$m\ddot{x} = -\gamma\dot{x} - kx + a(x - f) - (x - f)^3 \qquad (2.3)$$

$$\tau\dot{f} = bx - f$$

Upon scaling the parameters, the x and f parameters of the model have units of $\mathrm{N}^{1/3}$. Therefore, x in equation (2.3) is not the displacement of the hair bundle. However, under an assumption that C is a constant, x could be interpreted as a parameter that represents the bundle displacement. Similarly, for constant α and C, the f parameter has been interpreted as force. Note that each term in the first equation of (2.3) has the unit of a force as in the original equation of motion, equation (2.1). The t parameter has a unit of $\mathrm{N}^{-2/3}$ and has been interpreted as a scaled time.

Several mathematical models of hair-bundle motility proposed by [13] and [19], including the model used in this work, argue that, for an unloaded hair bundle in the absence of an additional mass, the inertial force term of equation (2.1) plays less important roles over the range of low frequencies corresponding to the dynamic range of a hair bundle as it is approximately in an overdamped limit. This is due to the large drag force experienced by *in vivo* hair bundle bathed in an extracellular fluid of the inner ear [13]. These models thus assume that the inertial force term is negligible, and the dynamic of hair bundles can be described by two 1st order differential equations.

$$\gamma\dot{x} = -kx + a(x - f) - (x - f)^3 + F \qquad (2.4)$$

$$\tau\dot{f} = bx - f$$

จุฬาลงกรณ์มหาวิทยาลัย
CHULALONGKORN UNIVERSITY

2.5 Predictions from the model

Results of equation (2.4) suggest that stiffness loading and a constant force, denoted by F_c, imposed on the bundle govern the spontaneous dynamics of hair bundle and its response to external forces. The system can undergo spontaneous relaxation oscillation under appropriate ranges of parameters (Figure 2.6A). Raising k reduces the amplitude and increases the frequency of the oscillation and also makes the oscillation more sinusoidal. The oscillator becomes bi-stable when the value of k is sufficiently low. Figure 2.6B shows the state diagram of a hair bundle that illustrates the behavior of its spontaneous dynamics at each operating point, determined by k and F_c. The lines that separate different states are associated with a bifurcation. The spontaneous oscillation regime is enveloped by a line of Hopf

bifurcation which consists of subcritical and super critical Hopf bifurcation. The bi-stable regime, on the other hand, is enclosed by a line of saddle-node bifurcation. For the scope in this thesis, we are focusing on the region around Hopf bifurcation.

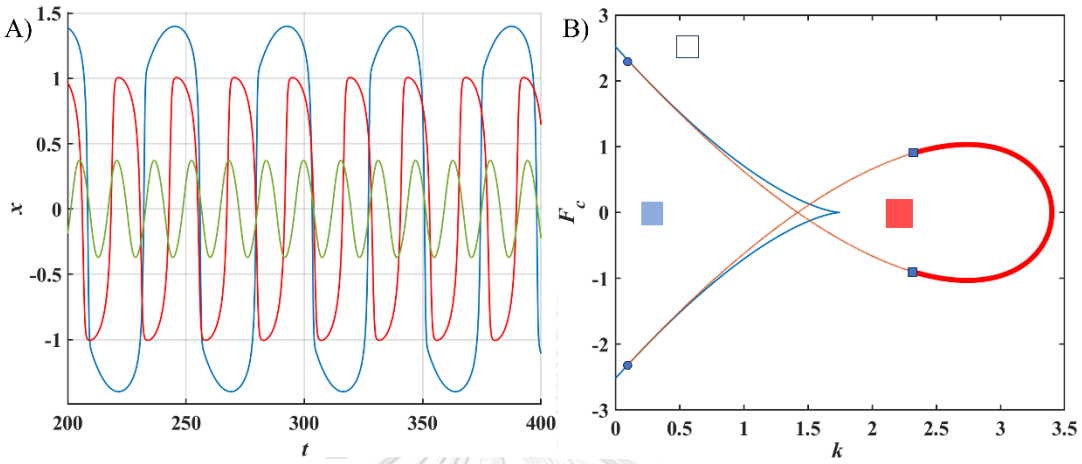

Figure 2.6 Spontaneous oscillation and state diagram of hair bundle. A) spontaneous oscillation of the hair bundle at $F_c = 0$ and $K_c = 1.8$ (blue), 2.5(red), 3.3(green). B) shows state diagram of hair bundle. The solid lines are bifurcations line separating the state of hair bundle into 3 regimes: spontaneous, quiescent, and bi-stable denoted by red, white, and blue square.

The responses of the system to external forces depend on the system's operating point relative to the bifurcation (Figure 2.7). The response to a sinusoidal force is quantified as the sensitivity defined as $|\chi| = |\tilde{x}|/|\tilde{F}|$ where $\tilde{...}$ denotes the Fourier component at the driving frequency. The sensitivity of a hair bundle poised near a Hopf bifurcation shows a peak across the forcing frequencies, with the highest sensitivity reduced and broadened when the system is displaced further from the bifurcation line into the quiescent regime (Figure 2.7B). For the response to step forces, the system near the line of Hopf bifurcation displays a damped oscillation during the transient response before moving to a steady state. When the system is poised further away from the bifurcation into the quiescent regime, the damped oscillation turns into an overdamped behavior (Figure 2.7C).

จุฬาลงกรณ์มหาวิทยาลัย
Chulalongkorn University

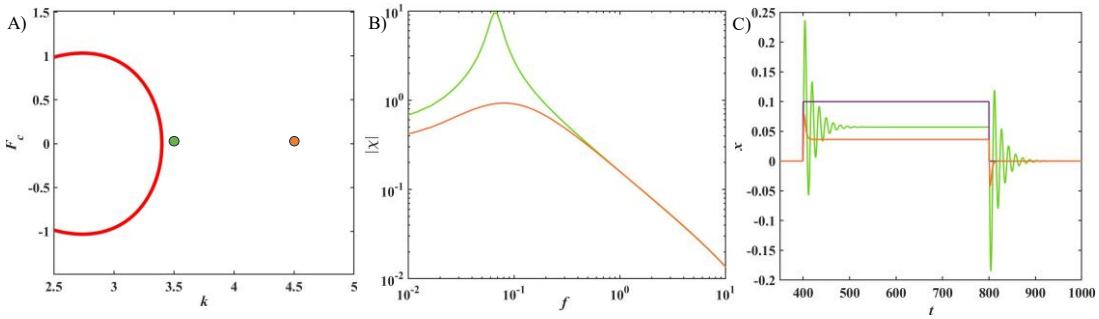

Figure 2.7 Responses of hair bundle to external force. A) A hair bundle's state diagram showing different operating points: near Hopf bifurcation (green point) and far from Hopf bifurcation (orange point). B) The response to sinusoidal force shows a sharp tuning when the system is near the bifurcation (green line). C) Hair bundle's displacement in response to step force (purple line) shows an underdamped oscillation when the oscillator is near the bifurcation (green line), and an overdamped motion when poised far from the bifurcation (orange line).

2.6 Phase portrait of a nonlinear oscillator

In this section, we describe the dynamics of a nonlinear oscillator as a trajectory on a phase plane consisting of x and f. From equations (2.4), we can find the solution to each of the differential equations when the time derivatives are set to zero. Each solution can be plotted in the phase plane as a line, termed nullcline, consisting of points at which the velocity of the system becomes zero. Figure 2.8A shows the nullclines obtained from equations (2.4) with $k = 2$ and $F_c = 0$. The interceptions between the two nullcline are called fixed points, at which both the displacement, x, and the internal parameter, f, of the system will be stationary. The fixed point can be either stable or unstable depending on the surrounding velocity vector field. The vector fields of the system are determined by the velocity $\dot{x}$ and $\dot{f}$ at any point of x and f from equation (2.2). The fixed point is stable when vector fields around fixed point are pointing into the fixed point while it became unstable when there are pointing out of the fixed point.

In our model, the fixed point is unstable when lies in the middle branch of the x-nullcline, shown in Figure 2.8. The system that originates at any point on the phase plane follows the velocity vector field and converges to a self-sustained oscillation and will not terminate at the fixed point. On the other hand, when the fixed point is situated on the left or right branch of the x-nullcline, it becomes stable and the system's trajectory drifts from its original state to the fixed point, resulting in a

quiescent solution. This can be achieved by introducing a constant force into the first equation.

On the other hand, when the stiffness parameter k is raised, the slope of the middle branch of the x-nullcline decreases. At the stiffness value corresponding to a point of supercritical Hopf bifurcation, the fixed point becomes stable as the surrounding velocity vector field spirals toward the fixed point.

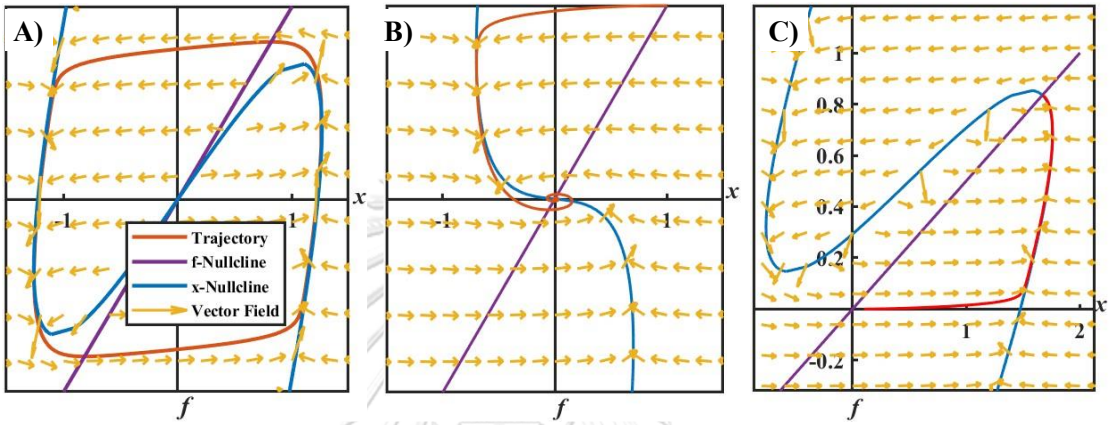

Figure 2.8 Phase portrait of equation (2.2) at 3 different sets of parameters. A) When k=2 F=0, the system shows spontaneous oscillation around an unstable fixed point. B) When k=3.6 F=0, the fixed point becomes stable, and the system is quiescent. C) When k=2, F=1, the fixed point is moved toward +x and +f directions. The fixed point is stable, so the system is quiescent.

จุฬาลงกรณ์มหาวิทยาลัย
Chulalongkorn University

Chapter 3
Methodology

In this chapter, we describe the details of the mathematical model of the motility of a single hair bundle and coupled hair bundles. The details of numerical simulations and parameter values utilized in the model are discussed. Finally, we present the calculation of the constant force experienced by each oscillator in the presence of coupling.

3.1 Mathematical model of a single hair bundle

The model employed in this work follows the work by D. Ó Maoiléidigh [2]. The dynamics of a single hair bundle are described by two dimensionless dynamical variables: x representing the displacement of the hair bundle, and an internal parameter, f, representing the force from a myosin motor complex [13]. Note that, as described in section 2.4, x could be interpreted as a scaled displacement that has a unit of $\mathrm{N}^{1/3}$. Moreover, we employed the limit proposed in [13] and [19] that the bundle moves at a sufficiently low frequency that the inertial force term became negligible.

$$\gamma\dot{x} = -kx + a(x - f) - (x - f)^3 + F_c + F \tag{3.1a}$$

$$\tau\dot{f} = bx - f \tag{3.1b}$$

จุฬาลงกรณ์มหาวิทยาลัย
Chulalongkorn University

where γ denotes a damping coefficient. The stiffness of the system is governed by k, corresponding to the total stiffness of all passive components of the bundle, and a representing the stiffness of the gating spring which can be modulated by the gating of ion channels. The oscillator is under a constant force, F_c, such as those imposed by the overlying structure, and a driving force from an incoming signal, F.

Equation (3.1b) describes the dynamics of the internal myosin-motor complex within the hair bundle as an overdamped oscillator. b represents the coupling strength between the bundle's displacement and the internal molecular motor, and τ represents a relaxation time of the internal motor.

3.2 Model of coupled hair bundles

Coupled hair bundles were modeled as two nonlinear oscillators, with subscription 1 and 2 denoting the first and second bundle of the system, respectively (Figure 3.1).

$$\gamma \dot{x_1} = -kx_1 + a(x_1 - f_1) - (x_1 - f_1)^3 + F_c + F - K_c(x_1 - Px_2) \quad (3.2a)$$

$$\tau \dot{f_1} = bx_1 - f_1 \quad (3.2b)$$

$$\gamma \dot{x_2} = -kx_2 + a(x_2 - f_2) - (x_2 - f_2)^3 + F_c + PF - K_c(x_2 - Px_1) \quad (3.3a)$$

$$\tau \dot{f_2} = bx_2 - f_2 \quad (3.3b)$$

The two oscillators are connected by a mechanical spring of stiffness K_c, whose extension is governed by Hooke's law. P denotes the coupling polarity. When the two hair bundles have identical polarity, $P = 1$, the extension of the coupling spring is determined by the difference in the oscillators' displacements (Figure 3.1A). On the other hand, for hair bundles with opposite polarities, whose coordinate systems are shown in Figure 3.1B, the extension of the coupling spring should be equal to the sum of the oscillators' displacements, i.e., $P = -1$.

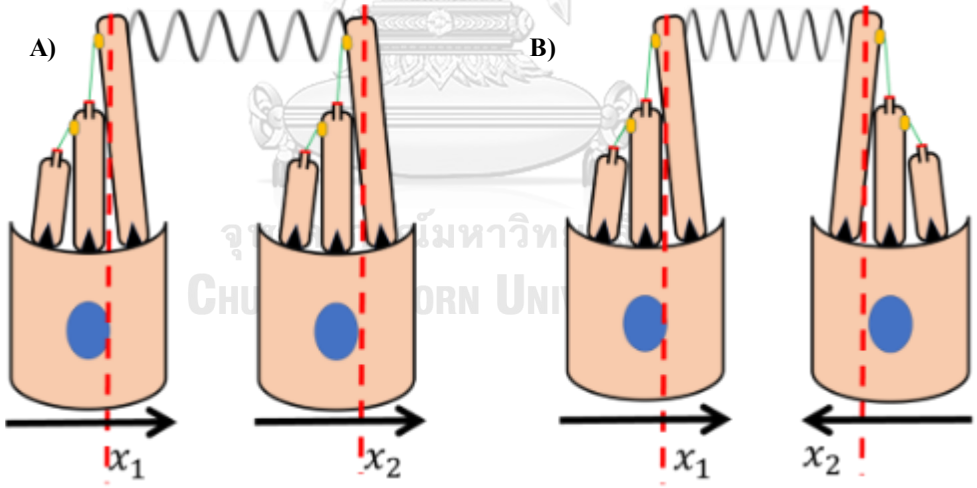

Figure 3.1 Schematic diagram of coupled oscillator. The Figure shows arrangement for identical polarity (A) and opposite polarity (B).

3.3 Numerical simulation and frequency analysis

Numerical integration of equations (3.2, 3.3) was performed in MATLAB using 4th order Runge-Kutta method with a time step of $\Delta t = 0.005$ for $t = 0 – 2100$. Note that t is a scaled time and thus does not have a unit of seconds. The oscillators' displacements during $t = 0 – 100$ were excluded from further analyses.

In this thesis, we investigated the responses of the coupled oscillators to sinusoidal forces and step forces. The sinusoidal force is defined as $F_{periodic} = A sin(2\pi f_d t)$, where f_d is the scaled frequency of driving force and A is driving force amplitude for $t \geq 0$. As t represents a scaled time, the parameter f_d also represents a scaled driving frequency.

The step force is defined as

$$F_{step}(t) = \begin{cases} A, & t > 400 \\ 0, & otherwise \end{cases} \tag{3.4}$$

where A corresponds to amplitude of force. The sign of A indicates the direction of the force relative to the first hair bundle (Figure 3.2).

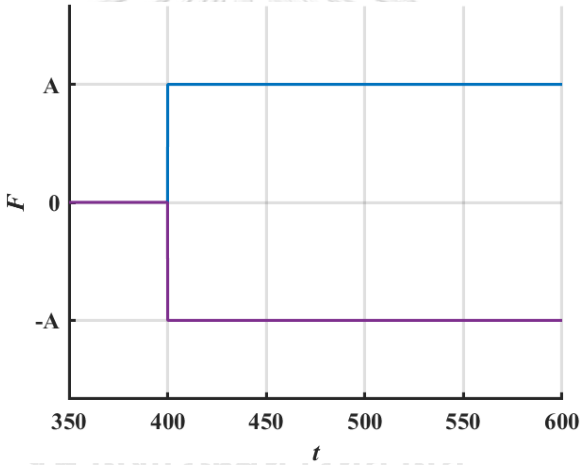

Figure 3.2 Step force to time. Figure shows the step force define in equation (3.4) in positive and negative direction with step size of A.

For the case of sinusoidal forces, we determined the amplitude of the hair bundle's oscillations by performing a discrete Fourier transform using Fast Fourier transform (FFT) of the bundle's displacement. The responses of each hair bundle at the driving frequency f were determined by linear response function defined as

$$|\chi(f_d)| = |\tilde{x}(f_d)|/|\tilde{F}(f_d)| \tag{3.5}$$

3.4 Parameters value

For simplicity, all parameters of the two hair bundles are assumed to be identical. This is based on *in vivo* hair bundles whose physical properties vary gradually along the length of the sensory epithelium. As a result, the characteristics of

neighboring hair bundles, such as their natural frequencies and stiffnesses, could be assumed to be identical. The constant parameters used in the simulations of equation (3.2-3.3) were referenced from [2]. The constant parameters were listed in Table 3.1

Table 3.1 shows the constant parameters.

Parameter	Value
γ	1
a	3.5
τ	10
b	0.5

The model employed in this work approximated the nonlinear force provided by the gating spring attached to mechanosensitive ion channels by a 3rd degree polynomial. Figure 3.3 shows the relationship between an external constant force and the oscillator's displacement, x. The oscillator displays a region of negative stiffness over a range of small x, due to gating compliance described in section 2.1. However, further away from the origin, the cubic term dominates, and the stiffness of the hair bundle increases continually. This contrasts with the findings from physiological measurements performed on hair bundles which reveal that hair bundle's stiffness saturates at a constant value when the bundle displacement exceeds ~10-20 nm [13]. The maximal stiffness observed experimentally corresponds to the sum of the passive stiffness of the bundle and the saturated stiffness of the gating spring. Therefore, our model is valid only for displacement not too far away from the origin, and we limit the amplitude of our driving forces to 0.1, a value that results in the response amplitude comparable to those of the spontaneous oscillations.

จุฬาลงกรณ์มหาวิทยาลัย
Chulalongkorn University

The values of coupling strength, K_c, used in this work were based on the estimation of *in vivo* coupling elements between hair bundles and their overlying structure. Experimental observations revealed that the coupling constant should be comparable to the total saturated stiffness of the hair bundle [20]. In our work, this could be approximated by the parameter a and k. Thus, we limited the range of the coupling strength within the orders of magnitude of a and k, i.e., the value of K_c employed in this work did not exceed 2. In a weakly coupling limit, we investigated

the oscillators dynamics under a coupling strength of approximately 10% of the maximal value, i.e., $K_c \sim 0.1 - 0.2$.

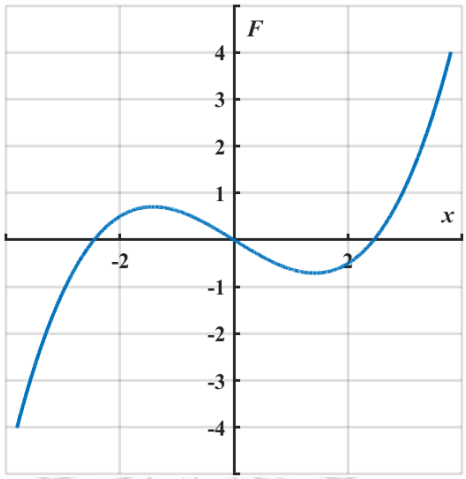

Figure 3.3 Force-displacement relation from the model..

3.5 Calculation of the constant force experienced by coupled hair bundles

The dynamics of a hair bundle are determined by its stiffness and the applied constant force (see Results section 4.1). Later in Chapter 4, we will show that coupling two oscillators with opposite polarities can drastically alter the constant force experienced by the individual oscillators. The reduced constant force results in the shift of the operating point of the oscillators closer to the line of Hopf bifurcation. Therefore, to faithfully compare the dynamics of driven coupled oscillators to those of a driven single oscillator, both systems must be at the same operating point by adjusting the constant force applied on the coupled oscillators. In this section, we present an analytical expression of the effective constant force exerted on a hair bundle in the presence of a coupling spring.

We solved for a steady state solution of equation (3.2-3.3) with no external force, thus $\ddot{x} = \dot{x} = \dot{f} = F = 0$. By substituting f_1 and f_2 from equation (3.2b) and (3.3b) into equation (3.2a) and (3.3a), respectively, one obtains.

$$0 = -kx_1 + a(1-b)x_1 - (1-b)^3{x_1}^3 + F_c - K_c(x_1 - Px_2) \qquad (3.6a)$$

$$0 = -kx_2 + a(1-b)x_2 - (1-b)^3{x_2}^3 + F_c - K_c(x_2 - Px_1) \qquad (3.6b)$$

Over the range of coupling constant, K_c, investigated in this work, the displacements of the two hair bundles remain nearly identical, i.e., $x_2 = x_1 = x$. For

coupling with identical polarities, $P = 1$, the coupling term is equal to zero and there is no alteration in the constant force exerted on the oscillators.

For opposite polarities, the sum of equations (3.6a-b) can be considered as a single 3rd degree polynomial equation.

$$0 = -(1 - b^3)x^3 + (-k + a(1 - b) - 2K_c)x + F_c \tag{3.7}$$

Let $\alpha = -k + a(1 - b) - 2K_c$ and $\beta = 1 - b^3$. The equation can be solved using Cardano's formula, if there is cubic equation $t^3 + pt + q = 0$ and $\Delta = \frac{q^2}{4} + \frac{p^3}{27} > 0$. There is one real solution $\sqrt[3]{-\frac{q}{2} + \sqrt{\Delta}} + \sqrt[3]{-\frac{q}{2} + \sqrt{\Delta}}$. This condition holds true when the system remains non-oscillatory, i.e., the oscillators are in a quiescent regime. The solution of equation (3.6) gives a stationary position of both oscillators.

$$x = \sqrt[3]{\frac{F_c}{2\beta} + \sqrt{\left(\frac{F_c}{2\beta}\right)^2 + \frac{\alpha^3}{27\beta^3}}} + \sqrt[3]{\frac{F_c}{2\beta} - \sqrt{\left(\frac{F_c}{2\beta}\right)^2 + \frac{\alpha^3}{27\beta^3}}} \tag{3.8}$$

The total force that applied on each oscillator is the sum of that of the constant force, F_c, and the force from coupling. Note that the coupling force is in the direction opposite to that of the constant force.

$$F_{eff} = F_c - 2K_c x \tag{3.9}$$

จุฬาลงกรณ์มหาวิทยาลัย
CHULALONGKORN UNIVERSITY

Chapter 4
Results

In this chapter, we present the dynamics of coupled hair bundles in the absence of an external force and their response to sinusoidal and step driving forces. The choices of driving forces are inspired by those experienced by hair cells *in vivo*. Hair cells in the auditory organs, such as the cochlea, detect sounds that exert sinusoidal forces on their hair bundles. On the other hand, hair cells in the vestibular organs, such as the semicircular canals which detect linear accelerations. We represent this type of stimuli by step forces with an abrupt onset.

Our investigation of the spontaneous behaviors of oscillators is based on several experiments conducted on hair cells *in vitro*. Typical experiments involve hair bundles that are separated from their surrounding structure and bathed in an appropriate solution. These free-standing hair bundles often exhibit spontaneous relaxation oscillations. [13].

4.1 Spontaneous dynamic

First, we verified the results of numerical simulations of our mathematical model by comparing the spontaneous dynamics of a single hair bundle with those that exist in the literature [2]. We numerically solved equation (3.1) in the absence of a driving force, $F = 0$. The spontaneous dynamics of the oscillator were investigated at different values of constant force, F_c, and the total stiffness of the bundle, k. Note that F_c represented the constant force imposed on *in vivo* hair bundles by their surrounding structure and was not regarded as a driving force as it was not imposed by the external stimuli.

จุฬาลงกรณ์มหาวิทยาลัย
CHULALONGKORN UNIVERSITY

We identified the oscillator as spontaneously oscillating when its root-mean-squared displacement exceeded an arbitrary threshold at 0.01. In agreement with previous studies, we found that the system can display a self-sustained oscillation (Figure 4.1A) over a range of appropriate values of F_c, and k. The range of parameters over which the system displayed spontaneous oscillations formed an enclosed area in the state diagram of k and F_c, as shown in Figure 4.1B. The oscillation profiles

resembled those of a relaxation oscillation, characterized by a slow movement followed by a fast swing.

Upon increasing k at a fixed value of F_c, the oscillation amplitude decreased while the frequency increased, and the oscillation profile became more sinusoidal. When the stiffness or constant force reached a value corresponding to the boundary of the enclosed area, the system underwent a Hopf bifurcation, and the oscillation amplitude vanished. These results were consistent with those presented in [2].

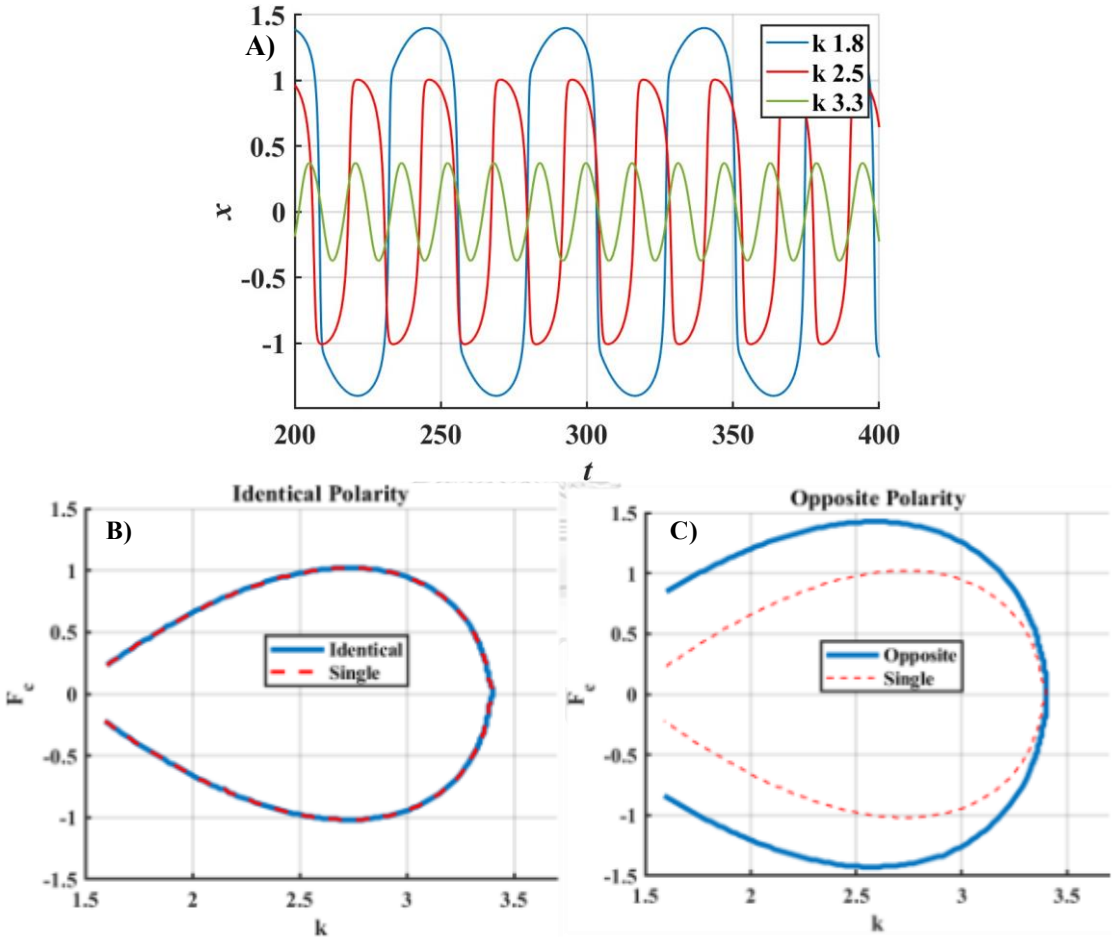

Figure 4.1 State Diagram for coupled oscillators. A) shows spontaneous oscillations of a single oscillator. Increasing K_c increases the oscillation frequency but decreases the amplitude of oscillation. B) shows the state diagram of single bundles (solid line) and coupled oscillators with identical polarity (dashed line). The lines separate the spontaneous oscillation regime (inside) from the quiescent regime (outside). C) presents the state diagram of coupled oscillators with opposite polarity. The data from coupled oscillators were obtained with $K_c = 0.2$.

Next, we investigated the spontaneous dynamics of coupled oscillators by introducing the coupling element into the equation (3.2). The coupled oscillators followed two possible configurations. Firstly, when the oscillators had identical polarities, the polarity parameter P was set to 1 as the extension of the coupling spring represented the difference in displacements between the two oscillators. For example, when both oscillators displayed equal displacements in their positive directions, the coupling spring remained at its equilibrium length and exerted no force on the oscillators. Conversely, coupled bundles with opposite polarities had the coordinate system of the second oscillator reversed compared to that of the first oscillator. Thus, when both oscillators displaced in their positive directions, the coupling spring was compressed by a distance equal to the sum of the oscillators' displacements, resulting in a coupling force towards the negative directions of both oscillators.

The spontaneous motions of two coupled hair bundles with identical polarity were studied at different values of k and F_c. It should be noted that the external constant force, F_c, was applied to both oscillators toward the same direction to simulate the force imposed by the overlying membrane on hair bundles. We found that coupling of hair bundles with identical polarity with $K_c = 0.1$ did not significantly change the oscillators' dynamics. The range of parameters over which the system displayed spontaneous oscillations remained virtually identical to that of a single oscillator. An increase in k also led to a gradual decrease in the oscillation amplitude, consistent with a Hopf bifurcation.

CHULALONGKORN UNIVERSITY

For coupling with opposite polarities, we applied an external constant force, F_c, in the same direction of both oscillators. Due to the reversed coordinate of the second oscillator, the forces appeared in opposite directions, as shown in Figure 3.1B. This force configuration was consistent with the electron micrographs of the membrane overlying *in vivo* hair bundles which pulled all bundles towards their channel-opening directions, corresponding to the positive direction of each oscillator in our model. We found that the range of parameters for spontaneous oscillations expanded in the direction of F_c (Figure 4.1C). The expansion of the state diagram was consistent with the shift of the line of Hopf bifurcation toward higher magnitudes of F_c, i.e., the system required a greater F_c to undergo a Hopf bifurcation. The extension was more

significant when the oscillators were more strongly coupled, with higher values of K_c. Notice that if $F_c = 0$, coupling did not affect the spontaneous dynamics of the oscillators.

We illustrated these effects by fixing K_c at 0.1 and $k = 2$, and plotted the peak-to-peak amplitude of the spontaneous oscillation at different values of F_c. Figure 4.2 shows that, when the system's F_c was below -0.95, the system remained in a quiescent state in the absence of external force. Upon a slight increase in F_c, the oscillation amplitude increased abruptly as a system underwent a subcritical Hopf bifurcation. The oscillation amplitude remained constant as the F_c magnitude increased. Until the F_c of system was above 0.95, system's oscillation amplitude experienced a sudden drop to quiescence as system underwent a subcritical Hopf bifurcation again. When compared to the oscillation amplitude of a single bundle at the same value of k, the plot illustrated that coupling the oscillators with opposite polarity shifted the bifurcation point toward a higher magnitude of F_c in both positive and negative directions while maintaining the same oscillation amplitude in the spontaneous oscillation regime, with respect to that of a single oscillator. This finding was consistent with the state diagram in Figure 4.1C.

Next, we sought an explanation underlying the expansion of the spontaneous oscillation regime in the state diagram by focusing on the set of parameters F_c and k at which the system became quiescent. This simplified our analyses as the oscillators were under a balance of two constant forces, i.e., the constant force F_c and the force from the coupling spring (Figure 4.3A).

จุฬาลงกรณ์มหาวิทยาลัย
CHULALONGKORN UNIVERSITY

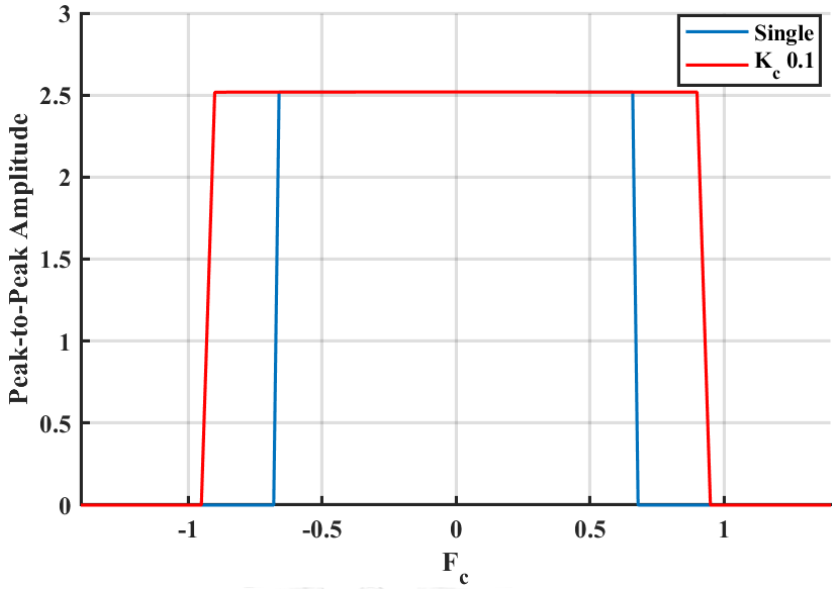

Figure 4.2 Peak-to-peak amplitude of coupled oscillators with opposite polarity (red) and a single bundle (blue) at $k = 2$. An abrupt increase and decrease in peak-to-peak amplitude correspond to the oscillators crossing a Hopf bifurcation.

The coupling force can be calculated from $K_c(x_1 - Px_2)$ which in case of opposite polarity, $P = -1$. In the absence of an additional force, the coupling force always acted in the direction opposing the applied constant force. This resulted in a reduction of the total constant force experienced by individual oscillators, given by $F_c - < K_c(x_1 + x_2) >_t$, where $\langle \dots \rangle_t$ denotes a time average. Consequently, the system was effectively under a weaker constant force and should appear closer to the line of Hopf bifurcation.

จุฬาลงกรณ์มหาวิทยาลัย
Chulalongkorn University

The reduction of the F_c was illustrated in Figure 4.3B. We plotted the total force experienced by the first oscillator as a function of the applied F_c. We found that, at the same value of F_c, the total force acting on coupled oscillators was lower than the force experienced by a single oscillator. As the value of F_c was reduced, the total constant force decreased linearly with a slope of 1, regardless of the coupling strength. This suggested that the coupling force, despite its growth with the value of K_c, remained at a constant value across F_c. We found that the quiescent regime of coupled oscillators always terminated at the total constant force of 0.66, a value corresponding to the bifurcation of a single oscillator. In other words, the state

diagram, as shown in Figure 4.1C, would remain unaltered from that of a single oscillator if the total constant force were plotted instead of F_c.

A further reduction of F_c shifted the system into the spontaneous oscillation regime where the coupling force varied with time. Our results showed that the coupling force simply served as an additional constant force that shifted the bifurcation of coupled oscillators. The shift of the line of Hopf bifurcation could be attributed to the reduction of the total constant force because the coupling force counteracted the applied constant force. More importantly, our results implied that the dynamics of the coupled oscillators can be regarded as two uncoupled oscillators under the effective constant force, with no alterations in the k of each oscillator.

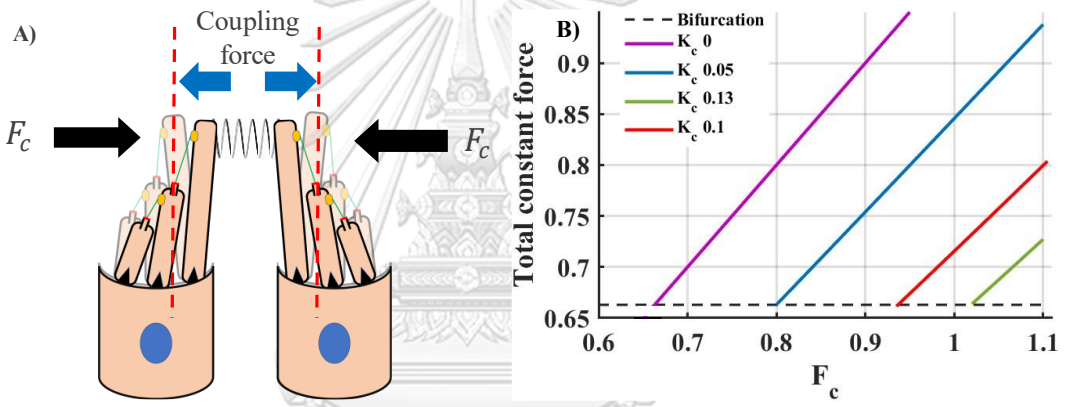

Figure 4.3 Force acting on individual oscillator. A) a diagram of coupled bundles with opposite polarity shows that under no external force the positive constant force F_c push both oscillators toward their respective positive displacement which contracted the coupling spring generated a coupling force in opposite direction to constant force for each oscillator. B) A plot of total constant force, $F_c - < K_c(x_1 + x_2) >$, as a function of F_c for a single oscillator and coupled oscillators with opposite polarity with $K_c = 0.05, 0.1, 0.13$. The quiescence regime of coupled oscillators was observed at $F_c >= 0.8, 0.94, 1.02$ for $K_c = 0.05, 0.1, 0.13$, respectively. At the bifurcation, the total constant force was always 0.66 for all K_c (dashed line). This value of total constant force was the same as that of a single oscillator.

4.2 Responses to sinusoidal force

Previous experimental studies have suggested that hair bundles in the auditory system become more sensitive to sinusoidal forces when operating as nonlinear oscillators near the verge of instability, such as a system near a supercritical Hopf bifurcation [5]. Under *in vivo* conditions, spontaneous oscillations of hair bundles

have not been observed. From the perspective of our model, this suggests that an oscillator should be poised in the quiescent regime near the line of a supercritical Hopf bifurcation. All results from numerical simulations presented in this section were obtained at the operating point of the system with k of 3.6 and F_c of 0.6, unless otherwise stated.

First, we illustrated the response of coupled oscillators with identical polarities. The response of the system to a driving sinusoidal force was quantified by a sensitivity (χ), defined as $|\chi(f_d)| = |\tilde{x}(f_d)|/|\widetilde{F}(f_d)|$. At a fixed driving force amplitude, A, of 0.1, the sensitivity of the coupled system displayed a resonance behavior with the peak's center frequency of f_d ~ 0.0675, and a quality factor of 30.72. The sensitivity was indistinguishable from that of a single oscillator (Figure 4.4A).

Upon varying the driving force amplitude, at a fixed frequency of 0.0675, near the resonant frequency in Figure 4.4B, the sensitivity plot exhibited two types of behavior. First, in the linear regime, a plateau in the sensitivity was observed over a range of low driving force amplitude. Second, in the nonlinear regime at higher driving force amplitude, the sensitivity followed a power law, $\chi \sim A\hat{}(-0.22)$. The negative exponent suggested a compressive nonlinearity of the oscillator [21]. As in Fig 4.4B, the sensitivity of coupled identical hair bundles was unaffected by the K_c and remained indistinguishable from that of a single bundle. These results indicated that there was no advantage of coupling hair bundles with identical polarity.

จุฬาลงกรณ์มหาวิทยาลัย
Chulalongkorn University

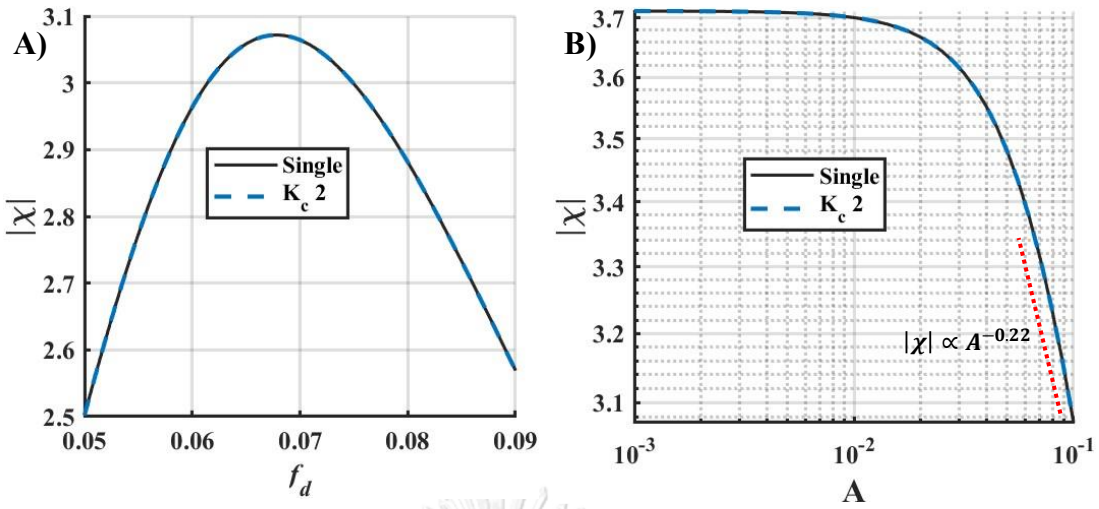

Figure 4.4 Sensitivity of coupled oscillators with identical polarity. A) a plot of sensitivity of coupled oscillators with identical polarity versus frequency of driving force, shows a resonance behavior with a peak frequency at 0.0675. The sensitivity is indistinguishable from a single oscillator. B) a plot of sensitivity vs driving force amplitude in logarithm scale shows two types of behavior, a linear response for lower driving force amplitude and nonlinear responses at higher driving force amplitude which portray the power law of -0.22.

Next, we investigated the response of coupled bundles with opposite polarities by changing the polarity parameter P in equation (3.2) to -1, with $F_c = 0.6$ and $k = 3.6$. At a fixed driving force amplitude at 0.1, the power spectrum of the first oscillator's displacement displayed a resonance behavior. However, the magnitude of the response was greatly enhanced compared to that of a single bundle. The resonant frequency remained relatively unchanged. The amplification became more pronounced with an increase in the K_c (Figure 4.5).

จุฬาลงกรณ์มหาวิทยาลัย
Chulalongkorn University

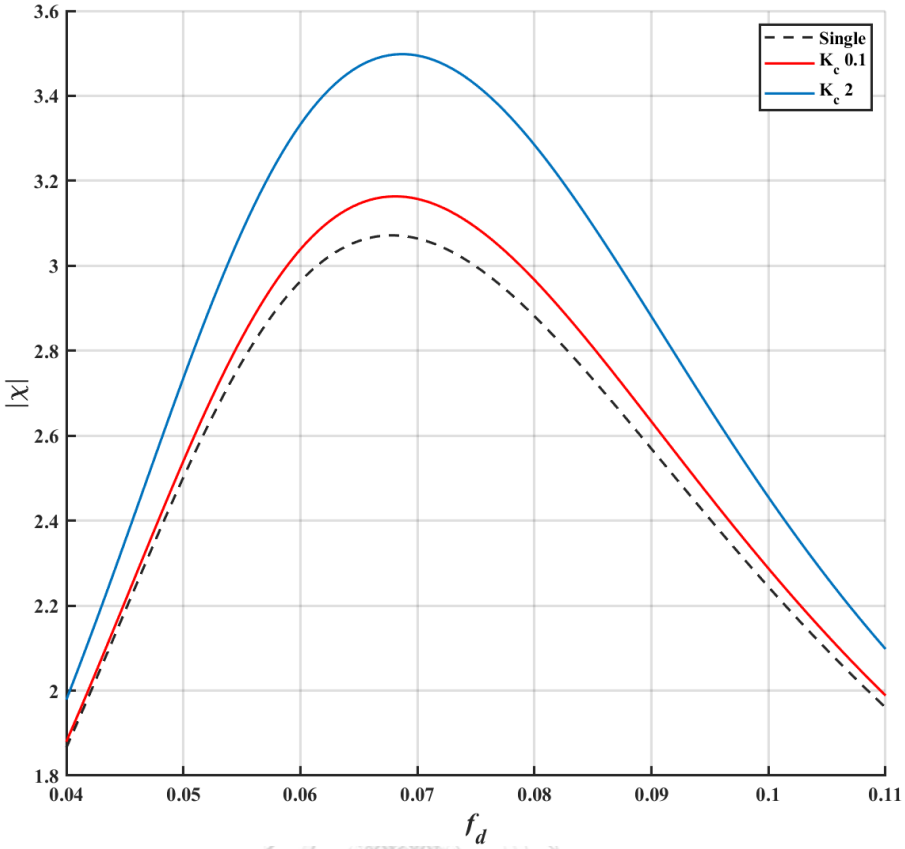

Figure 4.5 Sensitivity plot vs driving force frequency for coupled oscillator with opposite polarity for driving force amplitude of 0.1. The graph for every K_c shows a resonance behavior, with the peak frequency for K_c=0.1 and 2 slightly increased from an uncoupled oscillator. Increasing K_c also increases the overall sensitivity of coupled oscillators. The improved sensitivity could correspond to the shift in the line of Hopf bifurcation.

จุฬาลงกรณ์มหาวิทยาลัย
Chulalongkorn University

We hypothesized that the drastic enhancement in response due to coupling could be attributed to the shift of the line of Hopf bifurcation. As shown in the previous section, coupling reduced the effective constant force applied to the bundles, thereby shifting the operating point of the system closer to the line of Hopf bifurcation. This, in turn, enhanced the phase-locked amplitude of the response.

To reveal the roles of coupling, a faithful comparison between the responses of coupled, and uncoupled oscillators should be performed when the two systems were at the same operating point with respect to the bifurcation. To maintain the distance of the coupled system's operating point from the bifurcation, we increased the F_c applied to the oscillators in the presence of coupling. The magnitude of the F_c was calculated from equation (3.7). For example, to compare the response of a single oscillator with

$k = 3.6$ and $F_c = 0.6$ to a system of coupled oscillators with $K_c = 2$, the coupled oscillators should be under a constant force of F_c = 1.883.

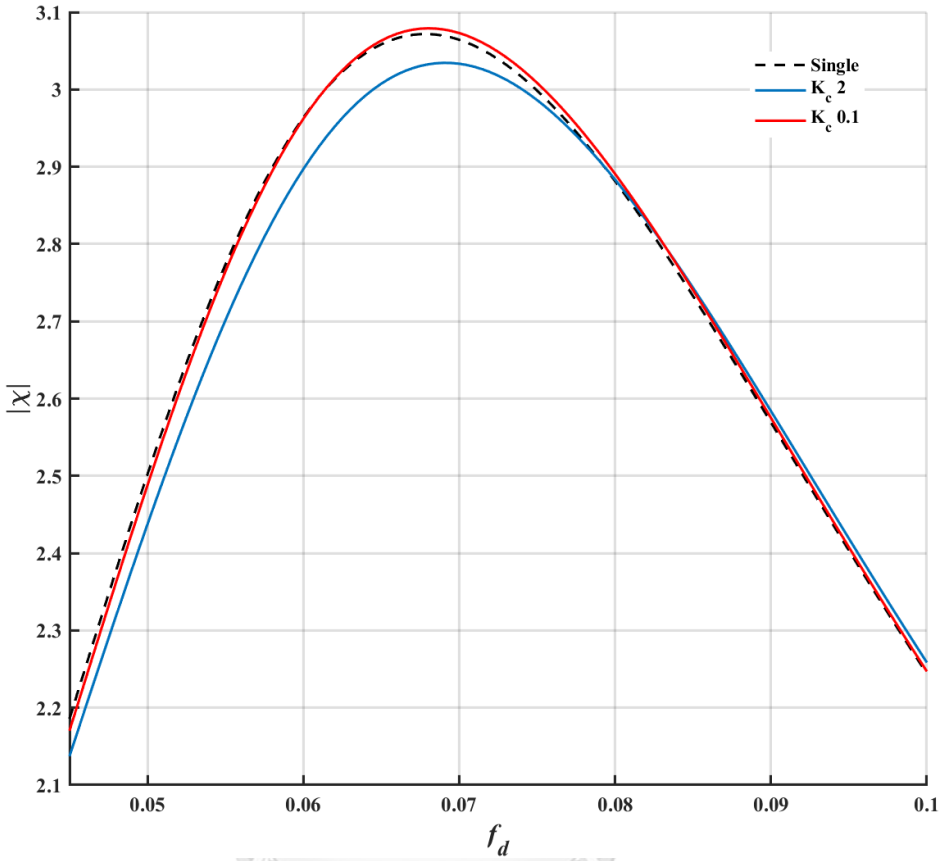

Figure 4.6 Sensitivity vs driving force frequency of coupled oscillators with opposite polarity at the same operating point at $k = 3.6, F_c = 0.6$. The driving force amplitude is fixed at 0.1. With K_c= 2, the sensitivity of coupled oscillators is lower than that of a single oscillator. This reduction is more pronounced at and below the resonance frequency. However, with K_c= 0.1, the sensitivity slightly increases around the resonance frequency.

After adjusting the constant force applied on the coupled oscillators with K_c equal to 0.1, the system's sensitivity across driving frequencies, with the driving force amplitude fixed at 0.1, was only marginally enhanced from that of a single oscillator, as shown in Figure 4.6. The amplification was more noticeable at a driving frequency slightly higher than the resonant frequency of the single oscillator. However, when the coupling constant K_c was set to 2, the overall sensitivity was significantly attenuated, particularly at frequencies f slightly below the resonance. This led to a shift of the response of the coupled oscillators towards a higher resonant frequency.

We found that the sensitivity of coupled oscillators with opposite polarities could be either enhanced or attenuated compared to that of a single oscillator, depending on the K_c. We fixed the driving frequency at a value near the resonance, 0.0675, and the forcing amplitude at 0.1, and varied the coupling constant K_c. Figure 4.7 illustrates that a range of sufficiently low values of $K_c < 0.4$ weakly enhanced the sensitivity. However, stronger coupling resulted in a monotonic decrease in sensitivity.

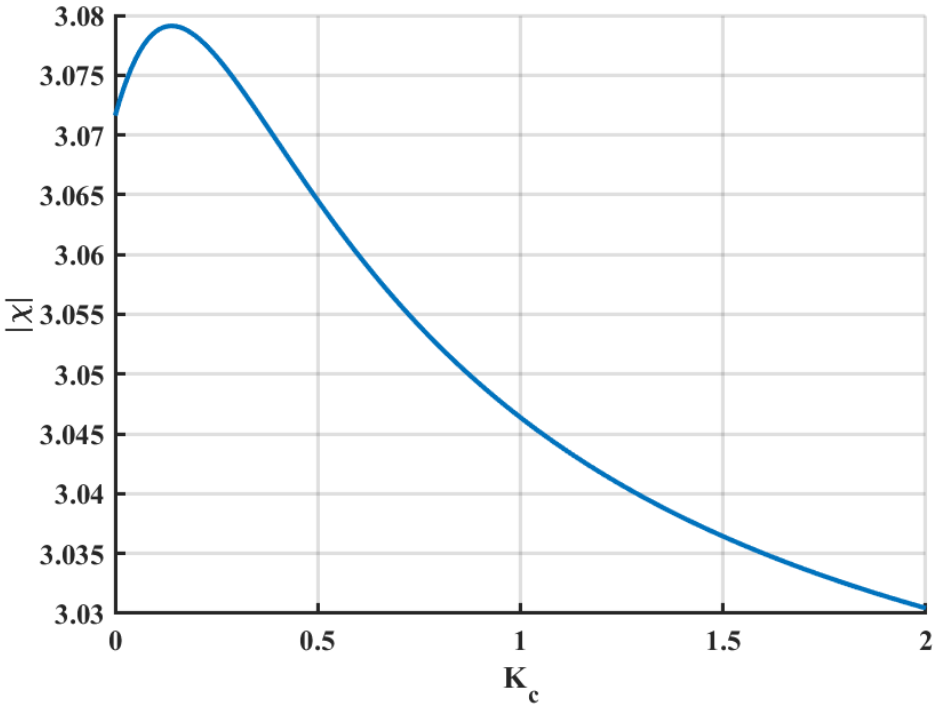

Figure 4.7 Sensitivity of coupled oscillators at frequency of 0.0675 and driving force amplitude of 0.1. For K_c below about 0.4, the sensitivity shows a small resonance behavior with a peak at K_c about 0.14. The sensitivity continues to decrease for $K_c > 0.4$.

The effects of coupling were also strongly dependent on the driving force amplitude. We illustrated this by plotting the sensitivities at K_c = 0.1 and K_c = 2 as a function of forcing amplitude at a fixed driving frequency f_d at 0.0675 (Figure 4.8A). The ratios between the sensitivities of coupled oscillators with opposite polarities to that of a single bundle in Figure 4.8B indicates that, for sufficiently strong driving force, $A > 0.01$, a high K_c resulted in an attenuation of sensitivity, while weak coupling slightly amplified the response. Interestingly, the trend reversed for forcing

amplitudes A below 0.01, where strong coupling slightly amplified the sensitivity, and weak K_c had no effect on the response.

To comprehend the impact of coupling on the sensitivity of two oscillators with opposite polarities, we analyzed the forces acting on each oscillator individually. Based on our previous finding, a coupled system can be perceived as two distinct oscillators influenced by the external force and the force arising from coupling. Consequently, each oscillator encountered three forces: the driving sinusoidal force, F_c, and the coupling force, represented by the coupling term in equation (3.2), $K_c(x_1 + x_2)$.

We illustrated that the dynamics of coupled oscillators with opposite polarities could be effectively described by a single oscillator influenced by the extracted coupling force and constant force. To compare the sensitivity of coupled oscillators with that of a single oscillator, we examined the response of coupled oscillators with opposite polarity under a constant force of 0.6 and a sinusoidal force of frequency 0.0675. In contrast, the single oscillator experienced no constant force and was driven by forces extracted from the coupled oscillators, including the driving force, the constant force, and the coupling force (Figure 4.9). Plotting the sensitivity across driving amplitudes revealed no distinction between the response of coupled oscillators and that of a single bundle subjected to the extracted forces. This allowed us to compare the response of two single oscillators, with one driven by a combination of the constant force and the coupling force.

จุฬาลงกรณ์มหาวิทยาลัย
CHULALONGKORN UNIVERSITY

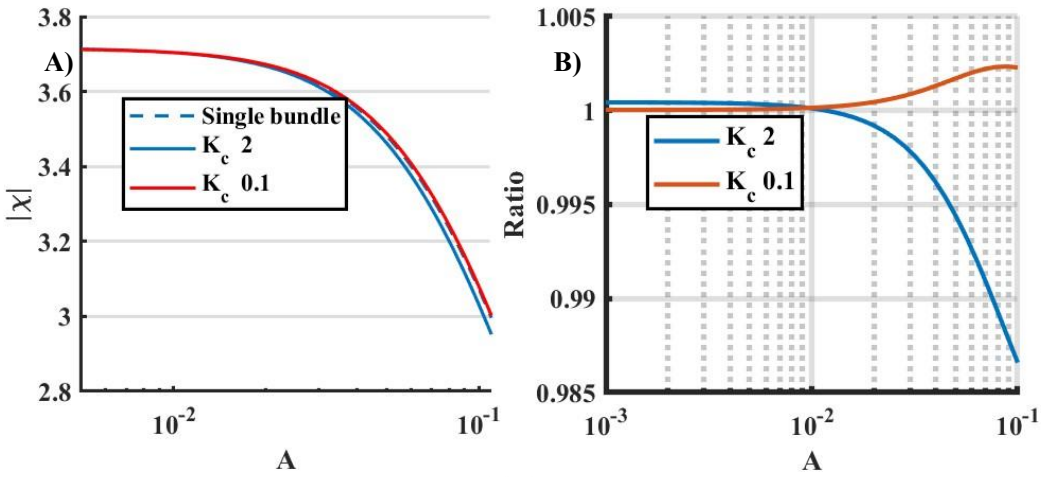

Figure 4.8 Plot of sensitivity versus driving force amplitude for coupled oscillators with opposite polarity at frequency of 0.0675. The sensitivity of coupled oscillators with $K_c = 2$ shows a reduction in nonlinear regime while $K_c = 0.1$ shows a marginal increase. B) shows a ratio between coupled oscillator and a single oscillator in A). Coupled oscillator with $K_c = 2$ had higher degree of reduction than $K_c = 0.1$ at higher force amplitude. However, as the force amplitude decreases, the degree of changes is reduced. For force amplitude below 0.01, the sensitivity of coupled oscillators with $K_c = 2$ shows a slightly amplification that do more than $K_c = 0.1$.

Next, we calculated the coupling force when coupled oscillators were under the driving force. Unlike the coupling force in coupled oscillators in quiescent state, the coupling force now oscillated around a non-zero offset of 1.275. This oscillation arose from the difference between two oscillators and was not purely sinusoidal owing to asymmetry of displacement of two oscillators. The oscillating coupling force provided the oscillator with additional periodic force, in addition to a constant force. To determine the frequency component of the coupling force that governed the sensitivity of the coupled oscillators, we performed a frequency analysis on the time trace of the coupling force using Fourier transform. The power spectrum revealed two predominant peaks: one at a frequency corresponding to the second harmonic of the driving force, and the other at zero frequency corresponding to a constant offset (Figure 4.10).

We postulated that the sinusoidal component of the coupling force was responsible for the alteration of sensitivity upon coupling. We investigated the dynamics of a single oscillator driven by a sinusoidal force at a frequency twice that of the driving frequency, in addition to the primary driving sinusoidal force. The amplitude of this 2nd harmonic force was set to match the oscillation amplitude of the

coupling force. Therefore, the total force exerted on a single oscillator was given by $F_{tot} = 0.1\sin(2\pi \cdot 0.0675 \cdot t) + 0.02\sin(2\pi \cdot 0.135 \cdot t)$, where the second term represented the sinusoidal component of the coupling force.

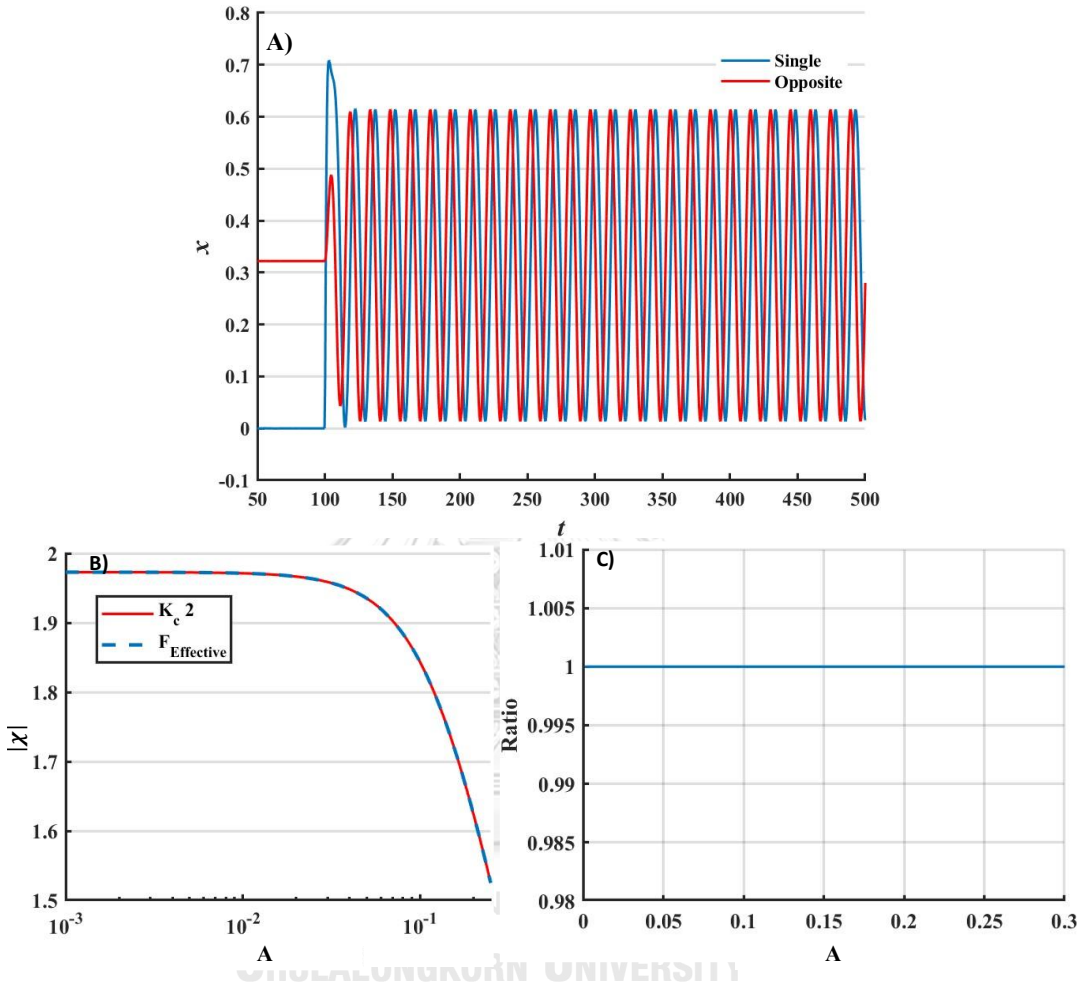

Figure 4.9 Comparison between the displacements of a coupled oscillator and a single oscillator driven by the forces experienced by an oscillator in coupled oscillators. B-C) shows sensitivity plot to driving force amplitude at frequency equal to 0.0675 and ratio between 2 cases which show an indistinguishable difference.

Figure 4.11 illustrated the power spectra of the response of three systems: coupled oscillators with opposite polarities, a single oscillator driven by one sinusoidal force, and a single oscillator driven by two sinusoidal forces, F_{tot}. A striking difference was observed at the second harmonic of the driving frequency, which was significantly suppressed for coupled oscillators with respect to those of the single oscillator. We hypothesized that the coupling force experienced by coupled oscillators

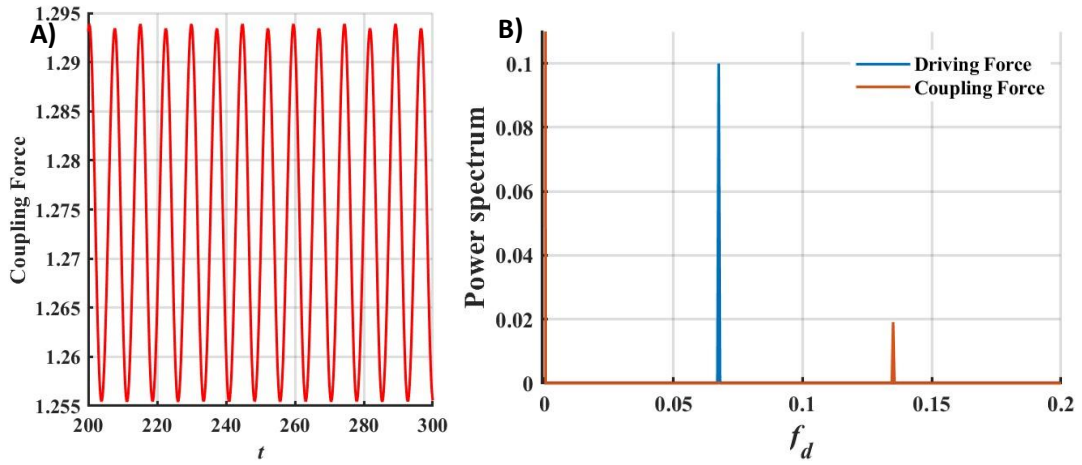

Figure 4.10 Coupling force. A) the coupling force as a function of time oscillates around an offset of 1.275. The oscillation amplitude varies between cycles due to an asymmetry in the motion of the two oscillators. B) the power spectrum of the coupling force shown in A) (red) compared to that of driven force (blue). The spectrum shows two frequency components, one at zero frequency and the other one at 0.135, which is equal to twice the frequency of the driving force. The peak at zero frequency corresponds to the offset of coupling force. The coupling force is extracted from coupled oscillators with $K_c = 2, k = 3.6, F_c = 0.6$ *driven by force amplitude of 0.1.*

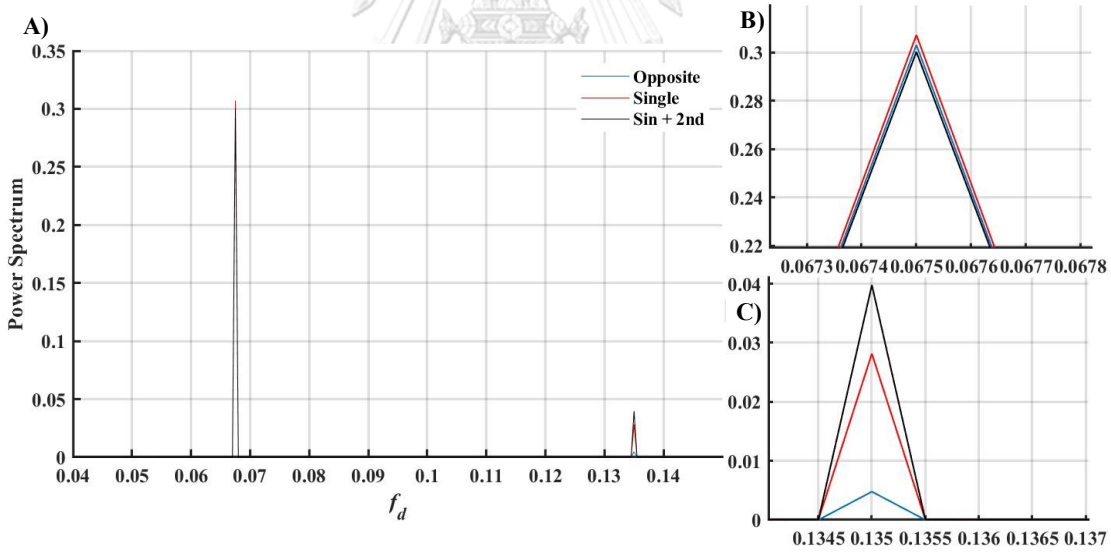

Figure 4.11 Power spectrum of responses from 3 different cases. A) consists of coupled oscillators with opposite polarity, a single oscillator under a driving sinusoidal force at frequency 0.0675, and a single oscillator under two driving forces at frequencies 0.0675 and 0.135. B) The peak at the driven frequency shows a slight reduction for opposite polarity and a single oscillator with additional 2nd harmonic force. C) The peak at a frequency equal to twice the driven frequency shows differences between opposite polarity which is suppressed while a single oscillator with additional 2nd harmonic force was enhanced compared to single oscillator.

could appear at a phase that led to a partial cancellation with the second harmonic response of the individual oscillators.

To illustrate the significance of the phase of the second harmonic force, we introduced a phase, φ, to the second term of the total force imposed on a single oscillator:

$$F_{tot} = 0.1\sin(2\pi \cdot 0.0675 \cdot t) + B\sin(2\pi \cdot 0.135 \cdot t + \varphi) \quad (4.1)$$

Here, B was the amplitude of the second harmonic force. We extracted the phase-locked amplitude and calculated the sensitivity at the driving frequency as shown in Figure 4.12. The results in Figure 4.12 indicated that the phase of the second harmonic force could either amplify or attenuate the sensitivity at the driving frequency f_d. The phase of the second harmonic force that amplified the response was between 1.1 rads and 4.3 rads, and this range remained unaffected by the amplitude of the second harmonic force.

Next, we verified that the phase of the coupling force of the coupled system could account for the alteration of the sensitivity. To relate the results from Figure 4.12 to the phase of coupling force, we needed to determine the phase of the sinusoidal component of the coupling force, i.e., the phase value in equation (4.1). We note that the phase, φ, in equation (4.1) represented the difference in the phases of the driving and coupling forces at time $t = 0$.

จุฬาลงกรณ์มหาวิทยาลัย
Chulalongkorn University

Firstly, we extracted both the driving force and the coupling force from an arbitrary time window, starting from $t = \tau$ to $t = \tau + \Delta t$. Next, we performed the Fourier transform of both forces and calculated the angles from the arguments of the complex Fourier component, $\tan^{-1}\left(Im(\tilde{F})/Re(\tilde{F})\right)$, at the driving frequency for driving force and at twice the driving frequency for coupling force. The obtained phase difference was, however, determined at time $t = \tau$. To retrieve the phase difference at $t = 0$, we rotated the angle of the two forces by subtracting the phase of the driving force by $2\pi \cdot 0.0675 \cdot \tau$, and subtracting the phase of the driving force by $2\pi \cdot 0.135 \cdot \tau$. The resulting phase difference was consistent with the definition in equation (4.1).

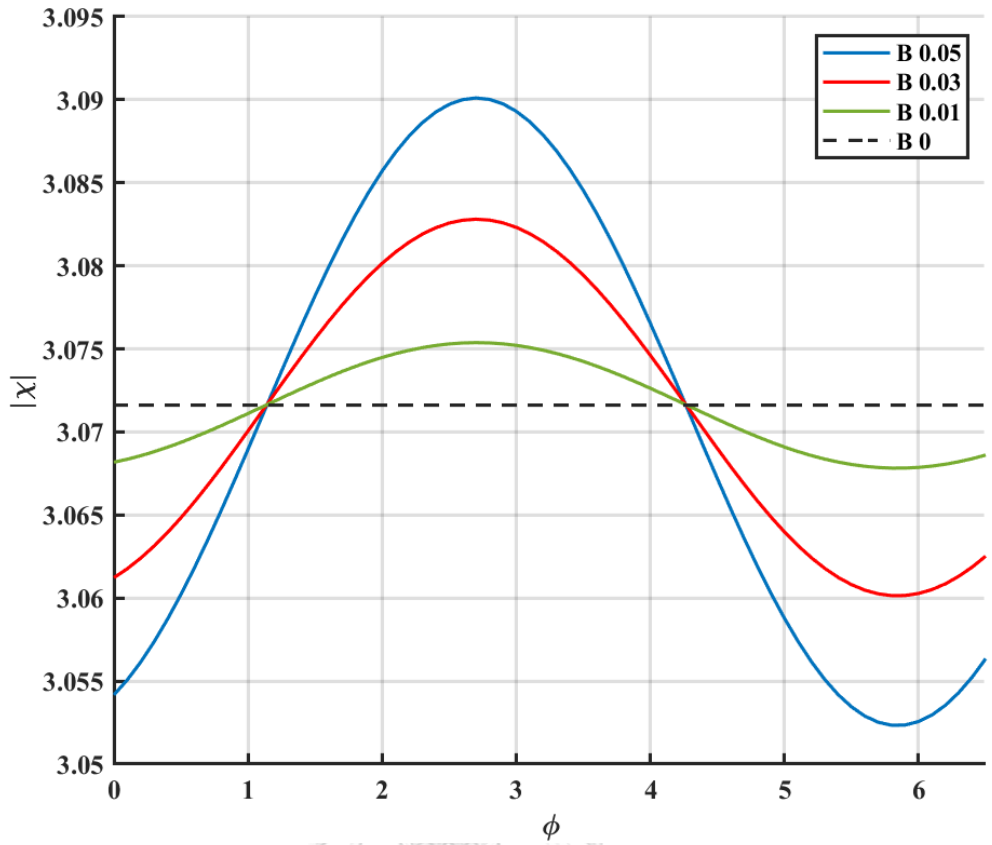

Figure 4.12 Sensitivity of a single oscillator vs phase of the second harmonic force for amplitude of the second harmonic force of 0.01, 0.03, and 0.05. With the presence of the second harmonic force, the sensitivity is amplified for phases between 1.1 and 4.3 and attenuated otherwise. Increasing the amplitude of the second harmonic force enhances the amplification and attenuation effects of the second harmonic force.

We found that the phase of the coupling force depended strongly on K_c while the driving force amplitude A had little effects. An increase in K_c from 0 to 2 led to a positive shift in the phase value from approximately 3.5 to 4.5 rads. On the other hand, increasing A only led to a slight enhancement in the phase of the coupling force. When compared to the range of phase values that led to an amplification of the sensitivity, as shown in Figure 4.13, we found that the phase values extracted from a coupled system at K_c = 2 was within the attenuation regime across driving amplitude. In contrast, the phase values obtained from the coupling constant at K_c = 0.1 was always within the amplification regime. Our results suggested that a strong coupling always attenuated the sensitivity while a weak coupling amplified the response across the entire range of A. This was consistent with the sensitivity ratio within the nonlinear regime shown in Figure 4.8. However, our findings could not explain the

sensitivity observed in the linear regime of Figure 4.8, in which a strong coupling slightly enhanced the response, whereas a weak coupling had no effects.

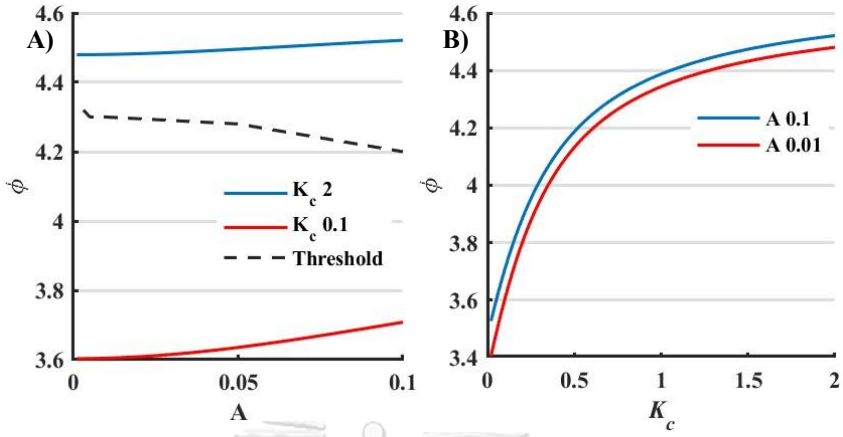

Figure 4.13 Phase of extracted coupling force. A) the phase of extracted coupling force vs driving force amplitude for $K_c = 2, 0.1$. The phase in both K_c is slightly reduced at lower driven force amplitude. In all range of driving force amplitude, the phase of coupling force with $K_c = 2$ is always fall in attenuation regime while for $K_c = 0.1$ the phase of coupling force is always in amplification regime. B) the plot between the phase of coupling force and K_c shows a significant decreased in phase with K_c which consistent across all considered range of driven force amplitude.

However, there was another parameter of the second harmonic force that might affect the sensitivity of coupled oscillator, the oscillation amplitude of the second harmonic force. As shown Figure 4.12, The oscillation amplitude of the second harmonic force affected the degree of amplification and attenuation from the phase of the second harmonic force. To determine the oscillation amplitude of coupling force, we measured the amplitude of coupling force at the frequency twice of that of driving force. Figure 4.14 shows the ratio between the amplitude of driving force and the amplitude of the second harmonic force from coupling force. The results showed that the amplitude of the second harmonic force decreased significantly with lower driving force amplitudes A and K_c. For example, the ratio reduced from 0.19 at A equal to 0.1 to ratio of 0.03 at A equal to 0.01. This trend also held true for different values of K_c. This result explained the varying degree of amplification and attenuation observed in nonlinear regime for K_c values of 0.1 and 2, as well as the diminishing effects at lower driving force amplitudes. Additionally, these results indicated that in the linear regime, there was minimal influence from the second harmonic force, which could not explain the slight amplification observed for $K_c = 2$ in the linear regime.

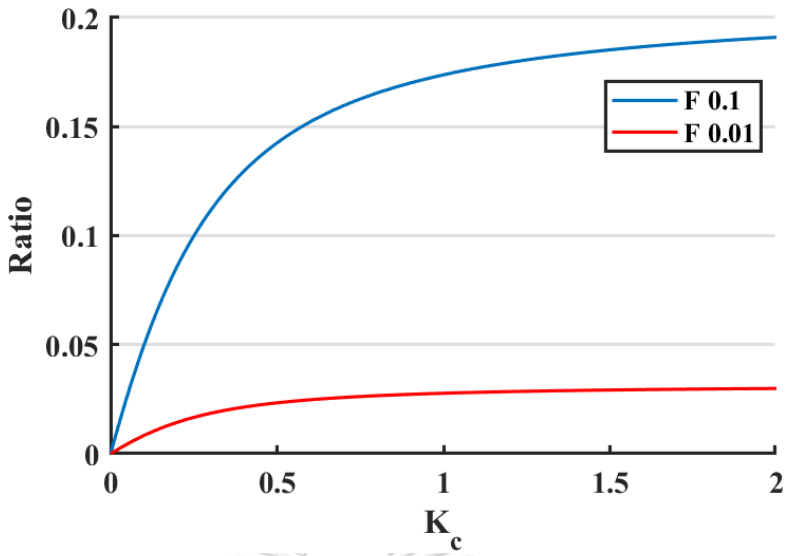

Figure 4.14 Ratio between the amplitude of the coupling force and the driving force. The ratio is lower with K_c and the driving force amplitude, indicating that the influence of the coupling force is minimized when there is a weak external force and weak coupling.

We also conducted a brief study on sensitivity at off-resonance frequencies. We choose the frequency of driving force f_a at 0.05 and 0.08 to represent the sensitive at lower and higher frequency than the resonance frequency, respectively. At both frequencies, the sensitivity to driving force amplitude exhibited both linear and nonlinear regimes, similar to that observed at the resonance frequency (Figure 4.15). However, at lower frequency, both $K_c = 0.1$ and $K_c = 2$ resulted in an attenuation of sensitivity in the coupled oscillator, whereas at the higher frequency, the coupled oscillator had minimal impact on the sensitivity.

จุฬาลงกรณ์มหาวิทยาลัย
CHULALONGKORN UNIVERSITY

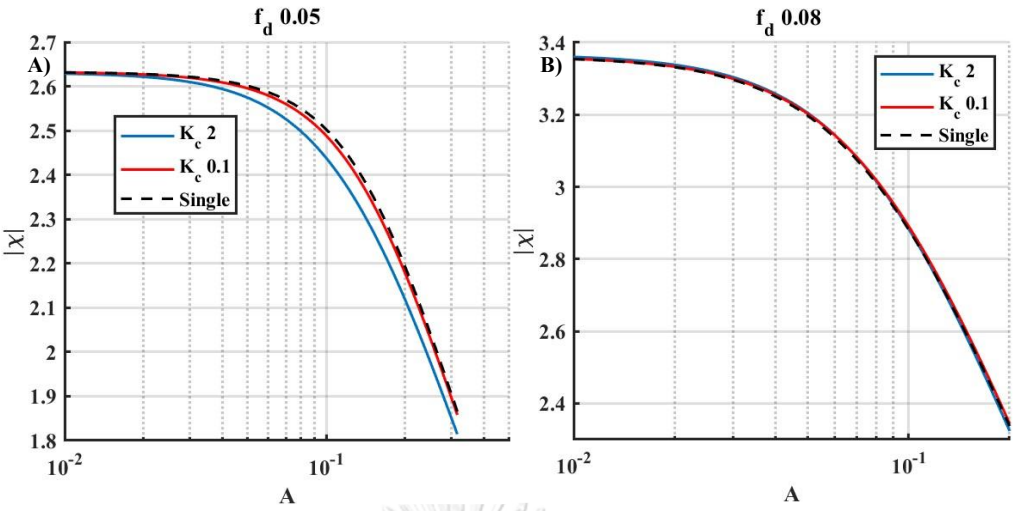

Figure 4.15 Sensitivity at off-resonance frequencies. For the driving frequency of 0.05 (A), the sensitivity of the coupled oscillator is reduced, even at K_c=0.1, compared to a single oscillator. On the other hand, for the driving frequency of 0.08 (B), the sensitivity of the coupled oscillator is unaffected.

4.3 Responses to step force

In this section, we investigated the dynamics of coupled hair bundles under a step force. The profile of this type of driving force represented a brief acceleration typically experienced by hair cells in the vestibular system. Previous theoretical studies of the nonlinear dynamics of hair bundles suggested that the vestibular hair bundles were suited for the detection of step force if poised near a subcritical bifurcation [5]. From the framework of our numerical model, this corresponded to an area near the upper or lower boundary of the enclosed area in the state diagram, as shown in Figure 4.1. Here, we choose the operating point of the oscillators to be in a quiescent regime near a subcritical Hopf bifurcation at $k = 2$, and F_c = 1.2, unless stated otherwise.

A step force was applied to both oscillators towards the same direction. Therefore, for coupled oscillators with opposite polarities, a step force in the positive direction induced a positive displacement of the first oscillator and a negative displacement of the second oscillator. Note that the orientation of this driving step force was different from a constant force, F_c, used to determine the system's operating point. The F_c evoked displacements of both oscillators towards the same direction, as illustrated in Figure 4.16.

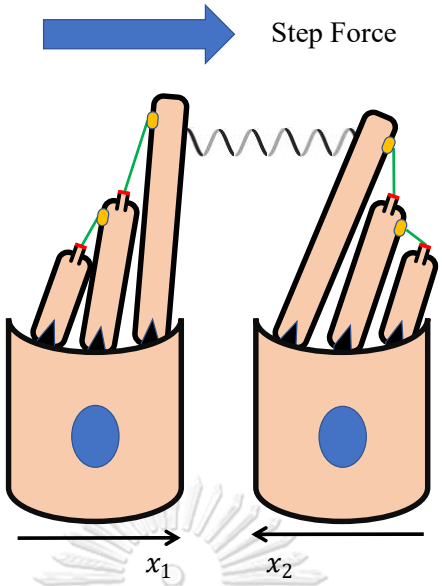

Figure 4.16 Schematic diagram of coupled oscillator with opposite polarity receiving a positive step force with respect to the first oscillator. The second oscillator, with its coordinate reversed, experiences a negative force.

Similar to the response to sinusoidal driving forces, the dynamics of coupled oscillators with identical polarity under a step force were indistinguishable from those of a single bundle as shown in Figure 4.17. The force in the positive direction caused an abrupt positive displacement, followed by a gradual drift in the negative direction toward an equilibrium point. The magnitude of this drift became less noticeable as the step size increased. On the other hand, a step force in the negative direction elicited a larger displacement, with respect to the motion evoked by a positive step force of the same magnitude. When the size of the step force exceeded a threshold value, approximately 0.3 in this case, the oscillators exhibited a large movement towards the negative direction and then abruptly swung back to a steady-state position, resulting in a 'twitch-like' movement. A larger step size could evoke a spontaneous oscillation, suggesting that the step force shifted the operating point of the system across the subcritical Hopf bifurcation.

The motion of coupled oscillators with opposite polarities elicited by step forces of different magnitudes was displayed in Figure 4.18. Note that the direction of a step force was determined based on the coordinate system of the first oscillator. For

example, a positive step force led to a positive displacement of the first oscillator and a negative displacement of the second oscillator.

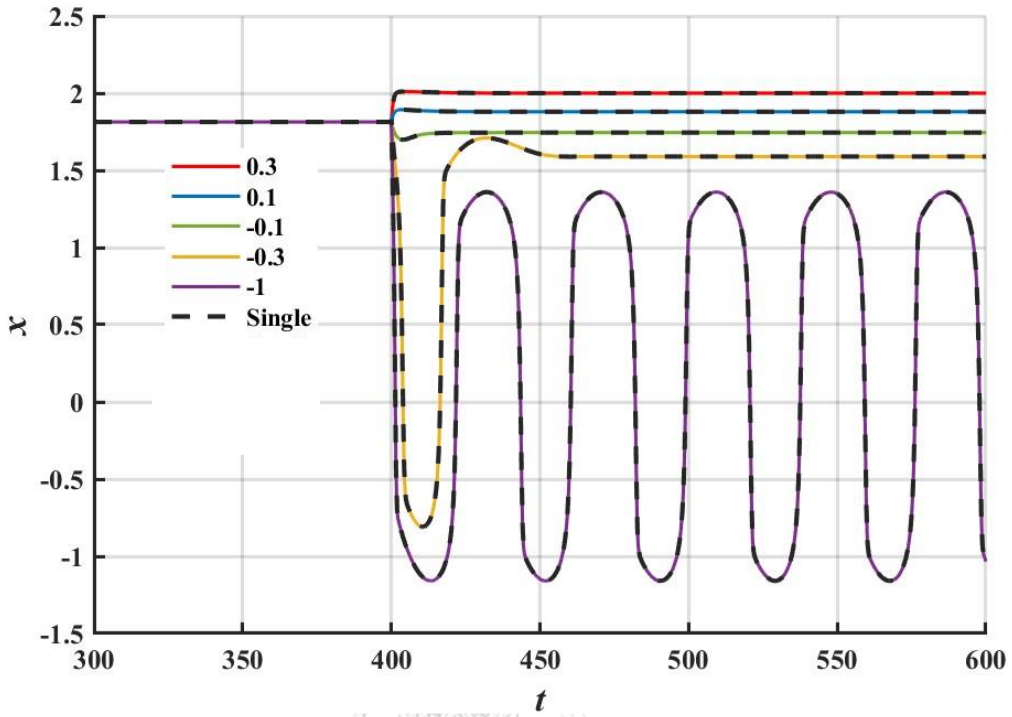

Figure 4.17 Responses to step force of coupled oscillators with identical polarity overlaid by responses from a single oscillator with the same external force. For a positive step force, the coupled oscillators response with an initial transient in positive direction slightly above steady displacement before slowly moving toward steady state. On the other hand, oscillators response to small negative force with larger initial transient compared to positive force. When the step size was large enough the oscillators display an abrupt large movement toward negative direction and swing back toward steady-state position. With a much larger step size in negative direction, the oscillators undergo a subcritical bifurcation and display a spontaneous oscillation.

The two oscillators displayed similar displacement profiles, but with different magnitudes. When a step force was applied towards the negative direction, the first oscillator displayed a significantly larger displacement compared to the second oscillator. A step size of 0.1 could induce a large twitch-like movement of the first oscillators, similar to what was observed in the case of a single oscillator or a coupled system with identical polarity. Meanwhile, the motion of the second oscillator underwent a more complex motion, with an additional step displacement superposed on the initial transient step.As the step size exceeded 0.3, the system displayed

spontaneous oscillation. While the oscillation profile of the first oscillator resembled a relaxation oscillation with a large amplitude, the second oscillator displayed a smaller-amplitude periodic motion at the same frequency. Note that this contrasted with the responses of a single oscillator and a coupled system with identical polarity which did not display a crossing of the bifurcation for step sizes below approximately 0.6. However, the amplitudes of the twitch-like response and the spontaneous oscillation in the first oscillator were smaller than those of a single oscillator. The reduction in the displacement of the first oscillator could be attributed to the coupling force that pulled it toward its positive direction.

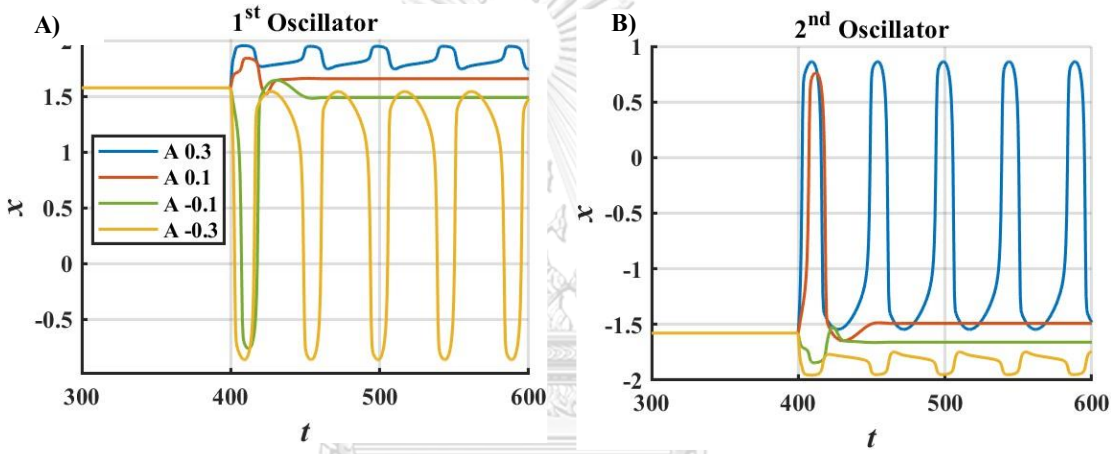

Figure 4.18 Responses of oscillators with opposite polarity. It should be noted that the displacement of the second oscillator is reversed to illustrate its displacement related to the first oscillator.

จุฬาลงกรณ์มหาวิทยาลัย
Chulalongkorn University

Next, we illustrated the motion of an individual oscillator as a phase portrait to understand its dynamics under a step force. A phase portrait represents the motion of an oscillator as a trajectory in the phase plane, which in our case consists of the displacement x and the internal parameter f. In general, a trajectory follows a vector field of velocity constructed from equation (3.1). The direction of the trajectory at any point in the phase plane is parallel to the velocity at that point.

To further visualize the dynamics of the oscillator, we calculated nullclines of equation (3.1a) and (3.1b) by solving the equations with the time derivatives, $\dot{x}$ and $\dot{f}$, set to 0. Therefore, an x-nullcline was composed of points at which the position, x, of the system became stationary. The intersection of the x-nullcline and the f-nullcline

was a fixed point, at which the oscillator was at rest. A fixed point was stable when the surrounding velocity vector field pointed toward the fixed point. In our case, stable fixed points appeared when the nullcline intersections were found on the two outer branches of the x-nullcline, resulting in a quiescent oscillator. On the other hand, an unstable fixed point was found in the middle branch of the x-nullcline, and the oscillator instead underwent a spontaneous oscillation resulting in a limit-cycle trajectory around the middle branch.

We first illustrated the trajectory of a single oscillator driven by a step force. Prior to the step force, the system was at rest at a stable fixed point, A, in Figure 4.19. An application of a negative step force of magnitude 0.3 suddenly changed the F_c and shifted the x-nullcline such that the new stable fixed point was now at point B. The oscillator then drifted from point A towards point B with the velocity determined by the velocity vector field. For small step sizes, this resulted in a small excursion in the phase plane, which corresponded to a slight dip observed in the time trace of the oscillator's displacement.

จุฬาลงกรณ์มหาวิทยาลัย
Chulalongkorn University

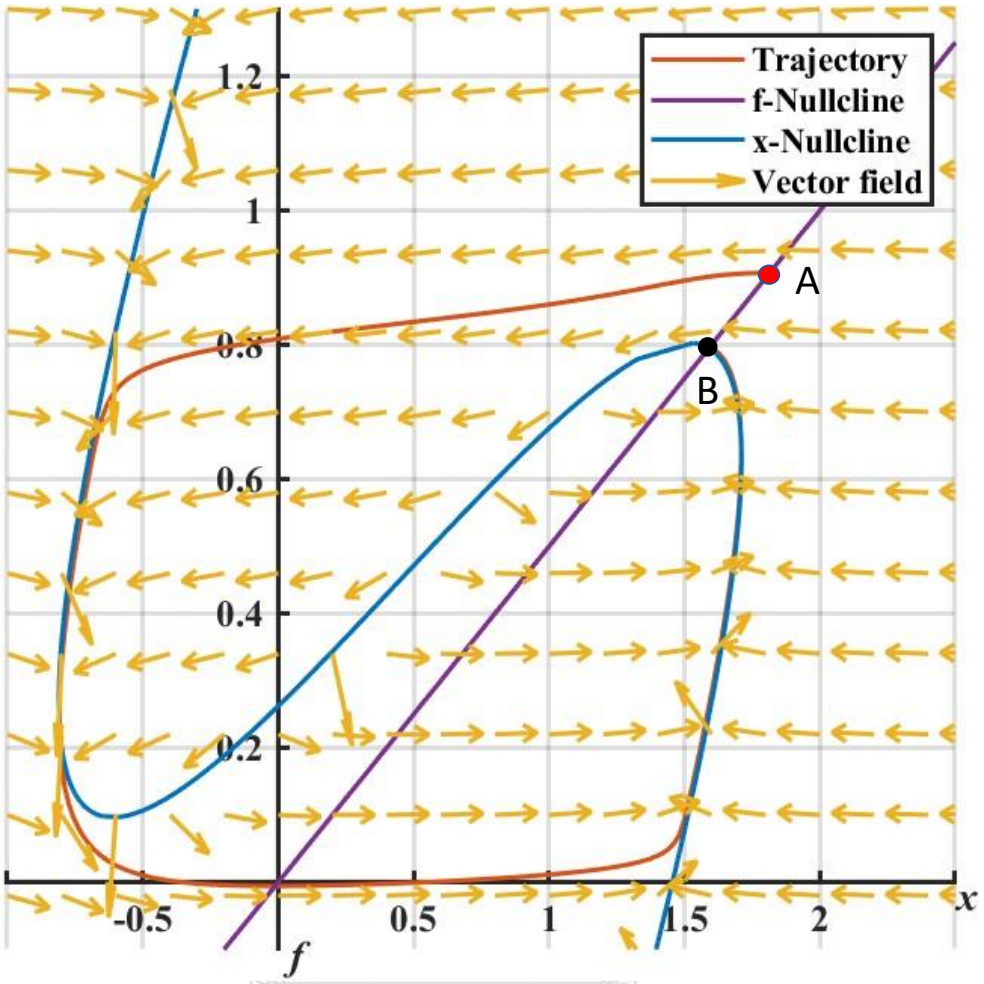

Figure 4.19 Trajectory of the oscillator receiving the step force of -0.3 from initial point A to final point B when the step force is applied. An oscillator moves toward point B with a velocity determined by vector field of point B. Note that the vector field only indicates the direction of velocity of system not the amplitude.

For negative step forces with a larger magnitude, the system was displaced across the separatrix, and the velocity field guided the system toward the left branch of the x-nullcline. The trajectory then tracked the x-nullcline back to the fixed point resulting in a large excursion which corresponded to the twitch-like motion of the oscillator. Upon a further increase in the step size to -0.6, the oscillator crossed the bifurcation, and the new fixed point was in the middle branch of the x-nullcline, becoming unstable. The oscillator then displayed a spontaneous oscillation following the velocity vector field. On the other hand, positive step forces always led to a small excursion of the system's trajectory as the system never crossed the separatrix (Figure 4.20).We applied this perspective to describe the motion of coupled oscillators with

opposite polarities. In contrast to a single oscillator, the x_1- and x_2-nullclines of the coupled system were also influenced by the coupling force. Figure 4.21A shows the total force, $F_c - K_c(x_1 + x_2)$, applied on each oscillator and coupling force. We found that the total force deviated from the applied step force as the coupling force exhibited a pronounced dip at the beginning of the step force.

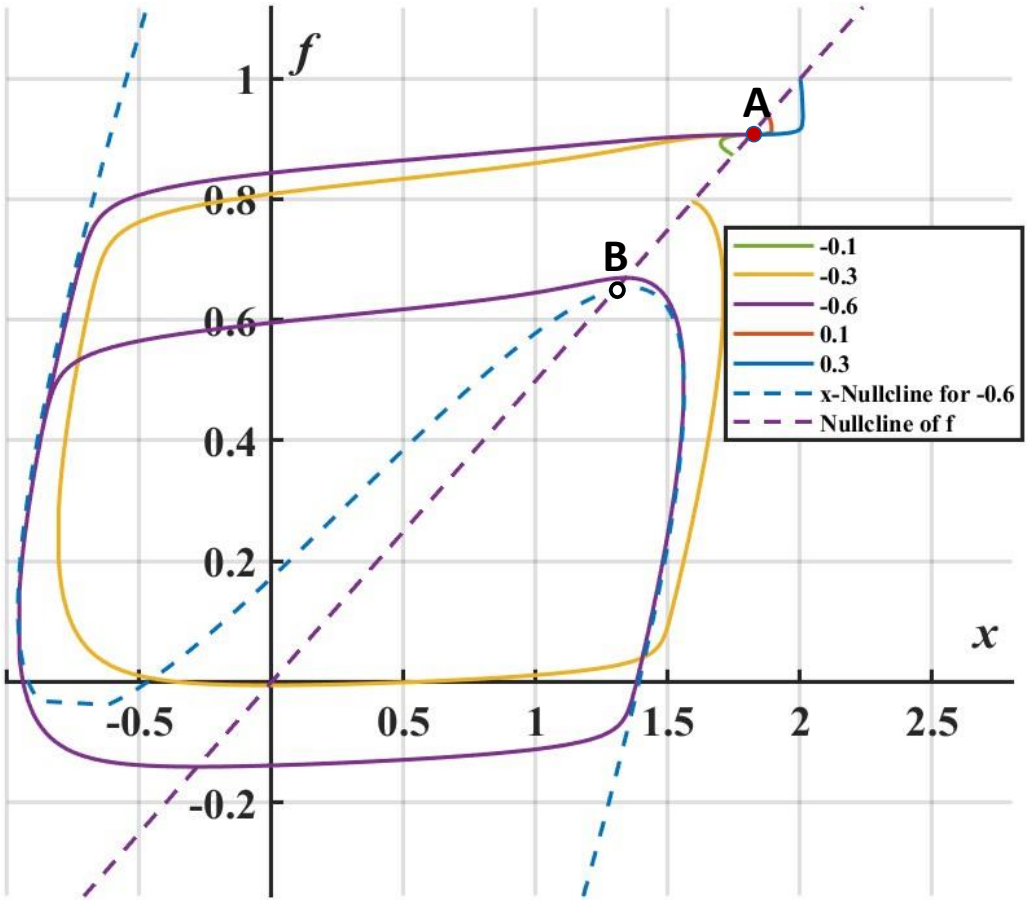

Figure 4.20 Trajectory of the oscillator shown in Figure 4.17 in phase plane. Before the force is applied, the oscillator is in steady state at position A. After the step force is applied, the oscillator drifts according to a velocity from vector field at new fixed point. For a step size of -0.6, the fixed point is in a middle branch of x-nullcline which is unstable. The oscillator then displays a spontaneous oscillation at point B.

Before a step force was applied, both oscillators remained at their initial fixed points. The two oscillators were subject to a total constant force of 1, with the coupling force magnitude of 0.33. Immediately after the beginning of a positive step force, the first oscillator's total constant force was changed to 1.31 and the x_1-nullcline shifted towards the positive x_1 direction, Line A in Figure 4.21B. The

oscillator drifted in the positive x_1 direction toward the new x_1-nullcline. As it approached the x_1-nullcline, however, the reduced coupling force raised the total constant force exerted on the first oscillator to 1.51. The x_1-nullcline was then shifted towards a more positive constant force to Line B in Figure 4.21B. The trajectory then followed the x_1-nullcline, corresponding to the complex motion exhibited by the first oscillator as shown in Figure 4.18A.

The second oscillator's total constant force was lowered to 0.70 upon the onset of the step force, leading to a shift of the x_2-nullcline in the negative x_2 direction (Line A in Figure 4.21C. As a result, the oscillator drifted to the new fixed points, exhibiting a higher velocity compared to the first oscillator and showing the onset of a twitch-like motion. The difference in velocities of the two oscillators caused their displacements to diverge and the coupling force decreased. This subsequently raised the total constant force exerted on the second oscillators to 0.91 shifting the x_2-nullcline to Line B. This made the amplitude of the twitch-like response lower than that of a single oscillator at the same F_c.

จุฬาลงกรณ์มหาวิทยาลัย
CHULALONGKORN UNIVERSITY

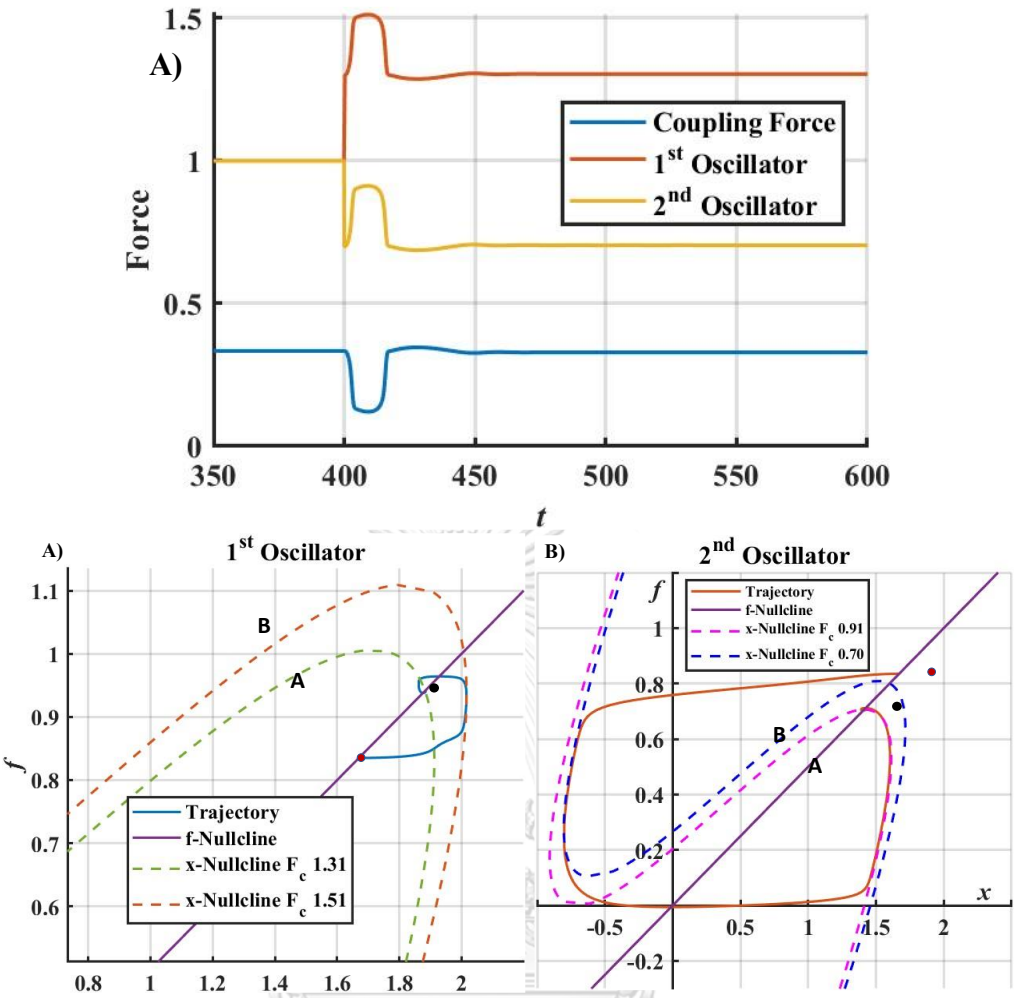

Figure 4.21 Trajectory and nullcline of each oscillator. A) shows coupling force and total forces acting on each oscillator over time. B-C) shows the trajectory of the first and the second oscillator and their x-nullcline at steady-state position and during the dip of coupling force, illustrating the shift of x-nullcline in relation to the dip of coupling force.

After the twitch-like response of the second oscillator, the force on both oscillators becomes stable near the value before a sudden transient of coupling force. Subsequently, both oscillators then moved according to vector field of this stable point.Finally, we illustrated the effects of coupling strength on the response to step forces. Since coupling can shift the operating point of the coupled oscillators with opposite polarities with respect to the line of Hopf bifurcation, we maintained the operating points at the same distance from the bifurcation as that of a single oscillator operating at $k = 2$ and $F_c = 1$ across all values of K_c. This was achieved by adjusting the value of F_c applied to coupled oscillators using equation (3.7).

Figure 4.22 shows the responses of both oscillators when subjected to positive step forces of magnitude 0.1 and 0.3 for which the system was expected to remain in the local vicinity of the fixed points, and to cross the separatrix, respectively. The K_c were varied at 0, 0.1, and 1. We found that a stronger coupling increased the amplitude of the transient response of the first oscillator while reduced the response amplitude of the second oscillator. At a step size of 0.3, a higher K_c also shortened the twitch-like response.

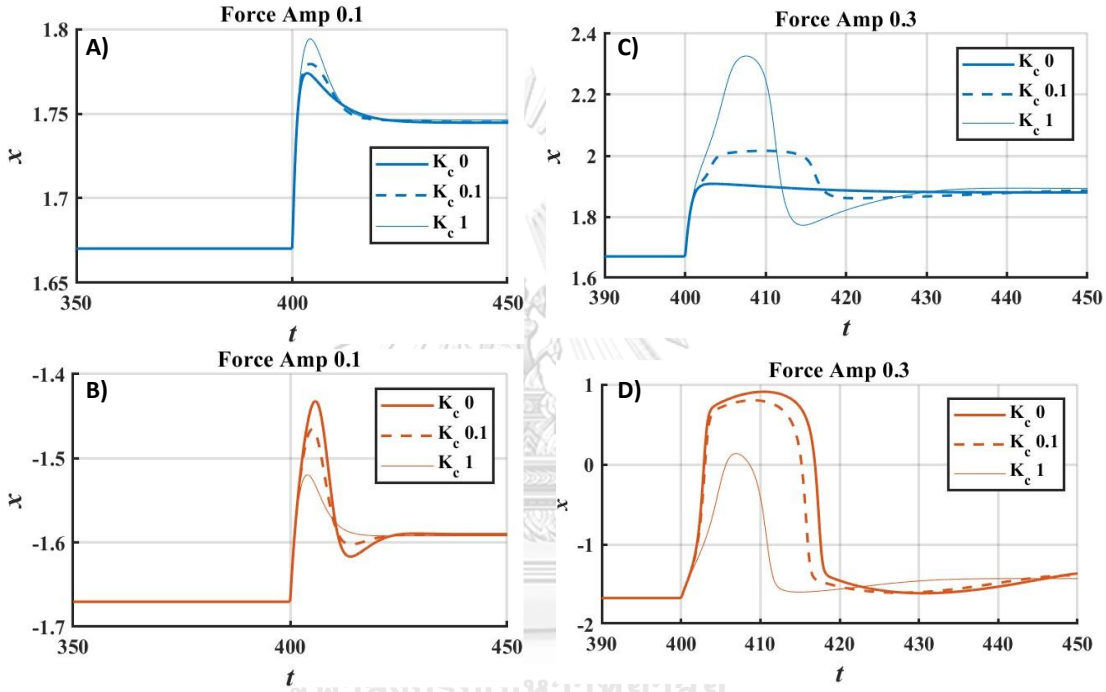

Figure 4.22 Responses of coupled oscillators to step force at higher K_c for step size of 0.1 (A, B) and 0.3 (C, D) respected to the first oscillator. In both step size, increasing K_c increases the amplitude of transient response for oscillator that received the force in positive direction while the amplitude is decreased in oscillator that received force in negative direction.

To understand the shortened transient response and the alterations in the response amplitude, we plotted the total constant forces exerted on the two oscillators and the coupling force, shown in Figure 4.23. We found that, for K_c = 1, the dip in the coupling force magnitude was sufficiently large that the total constant force exerted on the second oscillator could momentarily exceed its constant force in the absence of the driving force. Thus, it briefly experienced a positive step force, reducing its response in the negative direction. Moreover, we postulated that the positive shift of

x_2-nullcline during the reduced coupling force could make the second oscillator reach the left branch of the nullcline faster, resulting in the earlier recovery of the twitch-like response.

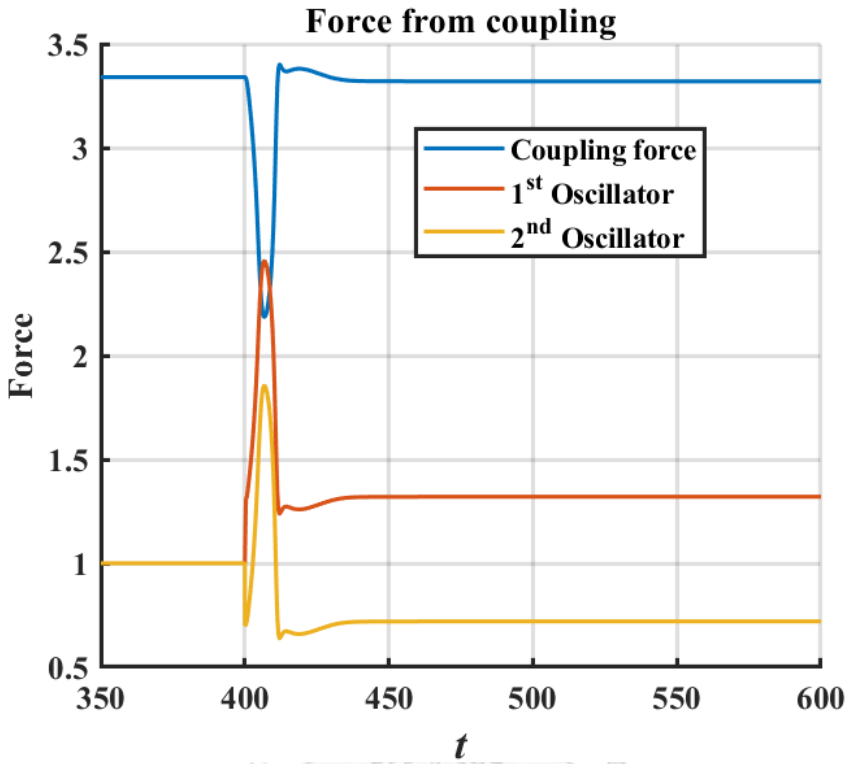

Figure 4.23 Coupling force and the total force acting on each oscillator for K_c= 1. The dip in the coupling force is higher compared to K_c=0.1, resulting in an increased total force on each oscillator. For the second oscillator, the increased force exceeds the value prior to the step force being applied. This indicates that the oscillator will reach the left branch of the x-nullcline faster, thereby reducing the swing distance and the time of the twitch-like response.

จุฬาลงกรณ์มหาวิทยาลัย
CHULALONGKORN UNIVERSITY

Chapter 5
Discussion and Conclusion

5.1 Discussion

Hair cells in certain sensory organs, such as the inner ear in lizards, the lateral line in fish, and the vestibular system in mammals, are coupled together with opposite polarity. In this study, we investigated the effects of coupled hair bundles with opposite polarity using a mathematical model of simple hair bundle motility that coupling through a mechanical spring. We investigated the dynamics of coupled oscillators in three scenarios: spontaneous dynamics, responses to sinusoidal forces, and responses to step forces.

By introducing the coupling spring into the system of two hair bundles with opposite polarity, the coupling spring imposed an additional force to individual hair bundle, influencing its dynamics. We showed that a single oscillator driven by the same forces experienced by each oscillator in coupled oscillators having the same responses to coupled oscillators. This suggested that a coupled system can be considered as a separated individual system driven by an additional coupling force.

The spontaneous dynamics of a single hair bundle are affected by the stiffness and constant force imposed on the hair bundle. We found that the state diagram of coupled bundles with opposite polarity resemble that in a single bundle with an expansion of state diagram in constant force direction. The force from the coupling spring, applied to the hair bundle in the opposite direction of the constant force, reduces the overall constant force acting on the hair bundle. This indicated that the coupling spring serves as another element that helped adjust the operating point of hair bundle.

The responses to sinusoidal force of coupled bundles with opposite polarity displayed a resonance behavior and a reduction of sensitivity following the power law at higher force amplitude similar to those of a single bundle but with a different degree of responses. By analyzing the coupling force while the coupled bundles were oscillating, we found that asymmetry of the oscillation of each bundles causing an

oscillation in coupling force at a frequency twice of that of a driving force. With high enough coupling strength, the second harmonic force attenuated the responses at the fundamental frequency. This effect was enhanced at higher driving force amplitude. This implied that the sensitivity of coupled hair bundle at nonlinear regime became more compressively nonlinear. This attenuation became more intense when the driving frequency was below the resonance frequency. For coupled bundles with weak coupling strength, the responses at resonance were slightly enhanced which may implied the benefit of coupling hair bundles when coupled with weak coupling.

We investigated the responses to step force of a single hair bundle by analyzing the phase portrait and studied the effects of coupled bundles with opposite polarity. For a single bundle, we found that the step force changed the hair bundle's constant force, causing the hair bundle to drift toward a new steady-state position through a velocity field determined by the vector field at new steady-state position. The hair bundle response to positive step force with initial transient with a small amplitude before moving toward steady-state position. For the responses to negative step, the hair bundle responded with higher amplitude than a positive force. When the step size crossed the separatrix, the hair bundle displays a twitch-like response with a larger amplitude than positive force. If the step size further increased, the hair bundle crossed the bifurcation and oscillate spontaneously. This implied that the characteristic properties of the responses, the responses amplitude, how fast the swing, was determined by the operating point of hair bundles. It also implied that the hair bundle that detecting the onset of step force prefer to have a lower stiffness which gave a larger swing at transient response. When coupling hair bundles with opposite polarity, the coupled bundles gain symmetry to direction of step force. In addition, we found that during initial transient response the coupling spring was extended which pull the hair bundle that received positive force forward while decrease the swing displacement for hair bundle that received negative force, which these effects were enhanced with coupling strength. This implied that the force from coupling force increased the transient responses to positive step force of hair bundle.

The arrangement of hair bundles with opposite polarity can be found in vestibular system such as literal line in fish and semicircular canals or saccule and

utricle in mammals [5]. These organs detect changes in forces or force accelerations. This arrangement is also found in auditory systems such as the inner ear in lizard which detects sound [6].

Our results suggested the advantages of coupling hair bundles with opposite polarities in signal detection. For the advantages in detecting sine waves, the second harmonic component may enhance the sensitivity of coupled hair bundle that coupling with a weak coupling. The reduction in sensitivity in frequency lower than fundamental frequency suggests that the coupled hair bundle may improve the frequency selectivity of hair bundles. Furthermore, the more compressive nonlinearity could increase the range of force amplitude hair bundles can detect and protect hair bundles from damage by reduction the responses to high-amplitude stimuli. By coupling hair bundle with opposite polarity also yield advantages in detecting step force. The symmetry of the coupled hair bundle helps the hair bundles to detect step the step force in both directions. The force from coupling force increased the transient responses to positive force, which promotes the opening of ion-channels, may enhance an onset detection of coupled bundled.

However, our model suggested that coupling hair bundles with identical polarity did not alter the dynamics of the bundles and gained no advantages over a single hair bundle in signals detections. This contrasts with the results from previous literature which suggested the benefit of coupled hair bundles [7, 8]. Our model also did not consider the effects of noise which affects the dynamics of hair bundle [19]. Additionally, we only studied a couple between two identical hair bundle.

In this work, we showed that the coupled hair bundle can be analyzed as a single hair bundle driven additionally by a coupling force which affected the dynamic and responses of the hair bundle. The results also suggested the benefits of coupled hair bundles with opposite polarity to the signal detection of hair bundle.

5.2 Suggestions and future work

The hair bundle in some organs are coupled with multiple hair bundle. [7, 8] suggest that the more hair bundle coupled together can further enhance the sensitivity

of hair bundles. We could extend the system to a higher number of hair bundles in the system. We could perform more extensive bifurcation analysis on the coupled hair bundles with opposite polarity. In this thesis, we only observed the displacement of the hair bundle. We could use the mathematical model of hair bundle motility from [13] to identify the open probability of the ion channel.

จุฬาลงกรณ์มหาวิทยาลัย
Chulalongkorn University

REFERENCES

1. Hudspeth, A.J., *Integrating the active process of hair cells with cochlear function.* Nature Reviews Neuroscience, 2014. **15**(9): p. 600-614.
2. Ó Maoiléidigh, D., E.M. Nicola, and A.J. Hudspeth, *The diverse effects of mechanical loading on active hair bundles.* Proceedings of the National Academy of Sciences, 2012. **109**(6): p. 1943-1948.
3. Salvi, J.D., et al., *Control of a hair bundle's mechanosensory function by its mechanical load.* Proceedings of the National Academy of Sciences, 2015. **112**(9): p. E1000-E1009.
4. Salvi, Joshua D., D. Ó Maoiléidigh, and A.J. Hudspeth, *Identification of Bifurcations from Observations of Noisy Biological Oscillators.* Biophysical Journal, 2016. **111**(4): p. 798-812.
5. Ó Maoiléidigh, D. and A.J. Ricci, *A Bundle of Mechanisms: Inner-Ear Hair-Cell Mechanotransduction.* Trends in Neurosciences, 2019. **42**(3): p. 221-236.
6. Fettiplace, R., *Diverse Mechanisms of Sound Frequency Discrimination in the Vertebrate Cochlea.* Trends in Neurosciences, 2020. **43**(2): p. 88-102.
7. Dierkes, K., B. Lindner, and F. Jülicher, *Enhancement of sensitivity gain and frequency tuning by coupling of active hair bundles.* Proceedings of the National Academy of Sciences, 2008. **105**(48): p. 18669-18674.
8. Prakash, R. and A.J. Ricci, *Hair bundles teaming up to tune the mammalian cochlea.* Proceedings of the National Academy of Sciences, 2008. **105**(48): p. 18651-18652.
9. Barral, J., et al., *Coupling a sensory hair-cell bundle to cyber clones enhances nonlinear amplification.* Proceedings of the National Academy of Sciences, 2010. **107**(18): p. 8079-8084.
10. Ahn, K.-H., *Enhanced signal-to-noise ratios in frog hearing can be achieved through amplitude death.* Journal of The Royal Society Interface, 2013. **10**(87): p. 20130525.
11. Zhang, T.-Y., S. Ji, and D. Bozovic, *Synchronization of Spontaneous Active Motility of Hair Cell Bundles.* PLOS ONE, 2015. **10**(11): p. e0141764.
12. Howard, J. and A.J. Hudspeth, *Compliance of the hair bundle associated with gating of mechanoelectrical transduction channels in the Bullfrog's saccular hair cell.* Neuron, 1988. **1**(3): p. 189-199.
13. Martin, P., et al., *Spontaneous oscillation by hair bundles of the bullfrog's sacculus.* J Neurosci, 2003. **23**(11): p. 4533-48.
14. Fredrickson-Hemsing, L., et al., *Dynamics of freely oscillating and coupled hair cell bundles under mechanical deflection.* Biophys J, 2012. **102**(8): p. 1785-92.
15. Roongthumskul, Y., J. Faber, and D. Bozovic, *Dynamics of Mechanically Coupled Hair-Cell Bundles of the Inner Ear.* Biophysical Journal, 2021. **120**(2): p. 205-216.
16. Manley, G.A. and C. Köppl. *Lizard SOAE Reflect an Active Process in the Hair-Cell Bundles*. in *ARO Abtract*. 2019.
17. Manley, G.A., et al., *In vivo evidence for a cochlear amplifier in the hair-cell bundle of lizards.* Proceedings of the National Academy of Sciences, 2001. **98**(5): p. 2826-2831.
18. Vilfan, A. and T. Duke, *Frequency Clustering in Spontaneous Otoacoustic*

Emissions from a Lizard's Ear. Biophysical Journal, 2008. **95**(10): p. 4622-4630.
19. Nadrowski, B., P. Martin, and F. Jülicher, *Active hair-bundle motility harnesses noise to operate near an optimum of mechanosensitivity.* Proceedings of the National Academy of Sciences, 2004. **101**(33): p. 12195-12200.
20. Strimbu, C.E., et al., *Correlated movement of hair bundles coupled to the otolithic membrane in the bullfrog sacculus.* Hearing Research, 2009. **256**(1): p. 58-63.
21. Eguíluz, V., et al., *Essential Nonlinearities in Hearing.* Physical review letters, 2000. **84**: p. 5232-5.

จุฬาลงกรณ์มหาวิทยาลัย
Chulalongkorn University

จุฬาลงกรณ์มหาวิทยาลัย
Chulalongkorn University

VITA

NAME	นายธนวัฒน์ งามพัตราพันธุ์
DATE OF BIRTH	26 มกราคม 2541
PLACE OF BIRTH	มุกดาหาร
HOME ADDRESS	22 ถ. ชาภูบาล ต.มุกดาหาร อ. เมืองมุกดาหาร จ. มุกดาหาร 49000
PUBLICATION	T Ngampattrapan and Y Roongthumskul 2023 The effects of hair-cell polarity on the dynamics of two coupled hair-cell bundles of the inner ear J. Phys.: Conf. Ser. 2431 012015

จุฬาลงกรณ์มหาวิทยาลัย
Chulalongkorn University